


March 2019

Conserved glycine residues control transient helicity and disorder in the cold regulated protein, Cor15a

Oluwakemi Sowemimo

University of South Florida, oluwakemi@mail.usf.edu

Follow this and additional works at: <https://digitalcommons.usf.edu/etd>

 Part of the [Cell Biology Commons](#), and the [Molecular Biology Commons](#)

Scholar Commons Citation

Sowemimo, Oluwakemi, "Conserved glycine residues control transient helicity and disorder in the cold regulated protein, Cor15a" (2019). *USF Tampa Graduate Theses and Dissertations*.
<https://digitalcommons.usf.edu/etd/7917>

This Thesis is brought to you for free and open access by the USF Graduate Theses and Dissertations at Digital Commons @ University of South Florida. It has been accepted for inclusion in USF Tampa Graduate Theses and Dissertations by an authorized administrator of Digital Commons @ University of South Florida. For more information, please contact digitalcommons@usf.edu.

Conserved glycine residues control transient helicity and disorder in the cold regulated protein, Cor15a

by

Oluwakemi Sowemimo

A thesis submitted as one of the requirements for the degree of
Master of science
with a concentration in Cell and Molecular Biology
Department of Cell Biology, Microbiology and Molecular Biology
College of Arts and Sciences
University of South Florida

Major Professor: Gary Wayne Daughdrill, Ph.D.
Kristina Schmidt, Ph.D.
Younghoon Kee, Ph.D.

Date of Approval: March 29th, 2019

Keywords:

Intrinsically Disordered Proteins (IDPs) , COR15A, LEA, NMR

Copyright © 2019, Oluwakemi Sowemimo

Acknowledgments

I would like to acknowledge Dr. Gary Wayne Daughdrill for allowing me to work in his lab. He is a great mentor, and without his enduring patience, guidance, wisdom, and resources, my project would have been impossible. I would like to thank Dr. Anja Thalhammer for her collaboration, which led to the provision of data crucial in publishing some parts of my project. To my committee members, Dr. Kristina Schmidt, and Dr. Younghoon Kee, thank you for guiding me from the beginning of my project to the end of my time at the University of South Florida's Cell & Molecular Biology program. I would also like to thank Dr. Wade M. Borchers for his hands-on training throughout my time in the program. To my lab mates, Emily, Melissa, Robin, and Serena, thank you for all the support over the last few years. Lastly, I would like to express my gratitude to the CMMB department for accepting me into their master's program as well as for their support, both financial and otherwise, throughout the program.

TABLE OF CONTENTS

<i>List of Tables</i>	<i>ii</i>
<i>List of Figures</i>	<i>iii</i>
ABSTRACT	v
CHAPTER 1	1
<i>Introduction</i>	1
1.1 Intrinsically Disordered Proteins (IDPs)	1
1.1.1 Structure and Function of IDPs	1
1.1.2 Nuclear Magnetic Resonance (NMR) Spectroscopy	2
1.2 Late Embryogenesis Abundant Proteins (LEA)	3
1.3 Cold Regulated Protein (COR15A)	3
1.4 Specific Aims	6
CHAPTER 2	7
<i>Identification and analysis of the amino acid residues that maintain the disordered structure of COR15A</i>	7
2.1 Rationale: Conservation of key amino acid residues in COR15A's amino acid sequence.	7
2.2 Effects of conserved glycine residues on the structure of COR15A.....	8
2.3 The effect of 20%TFE on the helical content of COR15A WT and Mutants.....	14
CHAPTER 3	21
<i>Examining the effect of increased helical content on the function of COR15A.</i>	21
3.1 Rationale	21
3.2 COR15AWT/MDMX solubility test.....	21
3.3 Carboxy Fluorescein assay	24
CHAPTER 4	28
DISCUSSION	28
4.1 The effect of glycine residues on the α -helical content of COR15A	28
Chapter 5	32
<i>Materials and Methods</i>	32

5.1 Preparing COR15A WT and mutant samples	32
5.1.1 Synthesis and sub-cloning	32
5.1.2 Transformations	32
5.1.3 Site directed mutagenesis	34
5.1.3.1 Polymerase chain reaction (PCR) set up	34
5.1.3.2 Polymerase chain reaction (PCR)	34
5.1.3.3 DpnI digestion	35
5.1.4 Transformation	35
5.1.5 Sub-cloning	36
5.1.5.1 Introducing the NdeI and XhoI cut sites into the plasmid (insert)	36
5.1.5.2 Digestion of the insert and pET28a vector using NDEI and XHOI	37
5.1.5.3 Agarose gel casting and sample extraction	38
5.1.5.4 Ligation	38
5.1.5.5 Transformation into NEB 5 α <i>E. coli</i> cells	39
5.1.6 Minipreps	39
5.1.6.1 Miniprep overnight cultures	39
5.1.6.2 Measuring plasmid DNA concentration and purity	41
5.2 Expression and purification of COR15A WT and mutant proteins	41
5.2.1 Transformation into BL21 (DE3) <i>E. coli</i> cells	41
5.2.2 Protein expression	41
5.2.3 Purification protocol for COR15AWT and mutant	44
5.2.3.1 Nickel affinity column purification of COR15A WT and mutants	44
5.2.3.2 Cleaving the 6x-histidine tag	46
5.2.3.3 Anion exchange chromatography	47
5.2.3.4 Size exclusion (SEC) chromatography	49
5.3 Polyacrylamide gel electrophoresis (SDS-PAGE)	50
5.4 Determining protein concentration	50
5.5 Nuclear magnetic resonance spectroscopy	50
5.6 Circular Dichroism	51
5.7 Carboxy fluorescein (CF) leakage assay	52
REFERENCES	54
APPENDICES	60
Appendix A: Chemical shifts tables for COR15AWT and mutants	61
Table A1. COR15AWT 0%TFE chemical shifts	61
Table A2. COR15AWT 20%TFE chemical shifts	63
Table A3. COR15 G68A 0%TFE chemical shifts	66
Table A4. COR15 G68A 20%TFE chemical shifts	68
Table A5. COR15 4GtoA 0%TFE chemical shifts	71
Table A6. COR15 4GtoA 20%TFE chemical shifts	73
APPENDIX B: COPYRIGHT INFORMATION	76

List of Tables

Table 1: % Helix prediction of COR15A in <i>Arabidopsis thaliana</i> and its homologs.....	10
Table 2: AGADIR % helix prediction of residues downstream and upstream from charged residues not involved in salt bridge formation.....	10
Table 3: Polymerase chain reaction steps as programmed into thermocycler.....	35
Table 4: Polymerase chain reaction steps as programmed into thermocycler.....	37
Table 5: Restriction digest scheme.....	38

LIST OF FIGURES

Figure 1. COR15A structure based on molecular dynamics simulations in vacuum.....	4
Figure 2. Change in membrane lipid structure due to freezing conditions in the absence and presence of COR15A.....	5
Figure 3. Sequence alignment of COR15A homologs in various plant species.....	9
Figure 4. AGADIR %Helix predictions for COR15AWT and single alanine substitutions.....	11
Figure 5. AGADIR %Helix predictions for CORWT and N- and C- terminal mutants.....	11
Figure 6. AGADIR %helix and IUPRED disorder predictions for individual residues in COR15A WT and mutants.....	12
Figure 7. 1H- 15N HSQC NMR spectra for COR15A WT and mutants in the absence of TFE.....	13
Figure 8. Residue- specific alpha-carbon secondary chemical shift and % helix plot for COR15A WT and mutants in 0% TFE.....	14
Figure 9. 1H- 15N HSQC NMR spectra for COR15A WT and mutants in the presence of 20%TFE.....	16
Figure 10. Residue-specific alpha-carbon secondary chemical shift and % helix plot for COR15A WT and mutants in the presence of 20% TFE.....	17
Figure 11. COR15AWT and mutants T2 plot.....	18

Figure 12. Far-ultraviolet (UV) circular dichroism (CD) spectra in buffer, 20 (v/v) % TFE and 12 M Ethylene Glycol for COR15A WT, G68A and 4GtoA.....	19
Figure 13. Solubility test plot for the supernatant samples.....	25
Figure 14. α -helical mutants reduce carboxy fluorescein (CF) leakage from vesicles.....	26
Figure 15. COR15A mutants have a higher helical content and are more protective than COR15A WT.....	30
Figure 16. This pET28a vector map showing the locations of the major components.....	33
Figure 17. COR15A expression test.....	44
Figure 18. Nickel column chromatogram. This figure shows the chromatogram of 2L COR15AWT on a Biorad NGC FPLC system.....	45
Figure 19. Nickel column fractions SDS-PAGE gel for COR15A WT.....	46
Figure 20. COR15A anion exchange chromatogram.....	48
Figure 21. COR15A SDS-PAGE anion exchange gel.....	48
Figure 22. COR15A size exclusion chromatogram.....	49
Figure 23. COR15A SDS-PAGE gel for the final stage of purification.....	50

ABSTRACT

COR15A is a cold regulated disordered protein from *Arabidopsis thaliana* that contributes to freezing tolerance in plants by protecting membranes. It belongs to the (LEA) Late Embryogenesis Abundant group of proteins that accumulate during the later stage of seed development and are expressed in various parts of the plant. During freezing-induced cellular dehydration, COR15A transitions from a disordered structure to a mostly α -helical structure that binds and stabilizes chloroplast membranes when cells dehydrate due to freezing. We hypothesize that increasing the transient α -helicity of COR15A under normal conditions will increase its ability to bind and protect chloroplast membranes when cells are frozen. To test this hypothesis, conserved glycine residues were mutated to alanine to increase α -helicity. NMR spectroscopy was used to examine structural changes of these mutants compared to wildtype in 0% and 20% TFE. The impact of these mutations on the stability of model membranes during a freeze-thaw cycle was investigated by fluorescence spectroscopy. The results of these experiments showed the mutants had a higher content of α -helical secondary structure than wildtype in 0% and 20% TFE. Increased α -helicity of the COR15A mutants improved membrane stabilization during freezing. Altogether, our results suggest the conserved glycine residues are important for maintaining the disordered structure of the protein.

CHAPTER 1

Introduction

1.1 Intrinsically Disordered Proteins (IDPs)

Intrinsically disordered proteins are proteins that do not form tertiary structures and may have some transient secondary structure [1, 2]. Proteins were formerly believed to require tertiary structure in order to have functions in cells, but a clearer understanding of intrinsically disordered proteins has shown that this is not always the case [1, 3-5]. IDPs serve a myriad of functions such as the formation of proteinaceous micelles, coupled folding and binding and flexible linkers [1, 2]. Compared to ordered proteins, some IDPs are more tightly regulated, and they evolve faster [4]. IDPs are most abundant in eukaryotes, however they are present in all organisms [6, 7].

1.1.1 Structure and Function of IDPs

The amino acid sequences of most IDPs are low in complexity because they are made up of repeats of specific amino acid residues or short amino acid motifs and they do not form long-range intramolecular interactions [4, 5, 8, 9]. IDPs contain a high number of charged and polar amino acid residues and few hydrophobic residues which prevents the formation of a hydrophobic core [1, 3]. IDPs are also known to have a high content of glycine and proline residues which destabilize alpha helices and beta sheets [8, 10]. Some intrinsically disordered regions (IDRs) are known to have a high frequency of insertions and deletions [4, 11-14].

The structure and dynamics of IDPs and IDRs have been studied using techniques such as circular dichroism (CD), Nuclear Magnetic Resonance (NMR) spectroscopy, and Dynamic

Light Scattering (DLS) [15, 16]. Of these methods, NMR is the most extensively used, and it is the method I used in my project [17].

1.1.2 Nuclear Magnetic Resonance (NMR) Spectroscopy

NMR spectroscopy is an indispensable method used in the characterization of IDPs. It gives residue specific chemical shift values. These chemical shifts are the resonance frequency of a nucleus in a magnetic field compared to a standard in the same magnetic field, and they are often used to determine the secondary structure of proteins [17]. alpha-carbon secondary chemical shifts are sensitive to helical structure and are also the most reliable chemical shifts used in determining helical populations in proteins [17]. Chemical shifts in the N-dimension are sensitive to the particular amino acid type. For example, glycine residues are always at the very top of the spectra in a ^1H - ^{15}N HSQC spectra, and alanine residues can be found towards the bottom of the spectra. The H-dimension is sensitive to the electromagnetic environment of each amino acid as influenced by its proximity to other amino acid residues [17, 18].

The analysis of the chemical shifts is often done with the use of chemical shift databases. Chemical shift databases such as BioMagResBank (BMRB) contain the chemical shifts of over 6000 proteins and peptides, and they help in understanding the relationship between chemical shifts and secondary structure [17]. Based on the data collected from these databases it was determined that, when in helices, $\text{C}\alpha$ and C' shifts are shifted downfield compared to their random coil values, and positive $\text{C}\beta$, N, H_N , and $\text{H}\alpha$ indicate beta sheets [17]. The random coil chemical shifts of a polypeptide state where the backbone phi and psi torsion angles of one amino acid are independent of neighboring residues [17]. In this project, we used isotropic chemical shifts to determine the helical content of a LEA protein called COR15A [17].

1.2 Late Embryogenesis Abundant Proteins (LEA)

LEA proteins are a family of proteins that accumulate during the later stage of seed development [7, 19]. They are expressed in various parts of plants when they are exposed to stressful conditions [7, 19, 20]. In the model organism *Arabidopsis thaliana*, 9 families of LEA proteins, made up of 51 protein encoding genes have been identified [7, 21, 22]. Most of these proteins are intrinsically disordered and they have low sequence complexity and repeat motifs [16, 21-23]. The various groups of LEA proteins have diverse functions and areas of localization and expression [7]. The nine groups are LEA 1-5, AtM, dehydrin, SMP (Seed Maturation Protein), and PvLEA18. Dehydrins, LEA 1, LEA 4, LEA5 and PvLEA18 are the intrinsically disordered LEA proteins, and most of the proteins that fall under these groups are proposed to be involved in the stabilization of macromolecules [23, 24]. The best characterized of these proteins is cold regulated protein 15A (COR15A) in *Arabidopsis thaliana*, and this is the main focus of this project [7, 22, 25]. A weak in-vacuo homology model, proposed by the Thalhammer group, unfolds rapidly in molecular dynamics simulations when hydrated. However, this model was useful for our current study and appears to depict the correct secondary structure of COR15A in the dehydrated state (**Figure 1**) [26].

1.3 Cold Regulated Protein (COR15A)

Cold regulated protein 15A is an intrinsically disordered plant protein in *Arabidopsis thaliana* that belongs to the late embryogenesis abundant family of proteins [19, 25]. COR15A is localized in the chloroplast, and after it is processed for chloroplast import, it is approximately 9.3 kDa [25]. In its native state (hydrated conditions) COR15A is intrinsically disordered, but during freezing-induced dehydration, COR15A accumulates helical structure and it has been proposed to form an amphipathic α -helix that is reversible upon rehydration [20, 26].

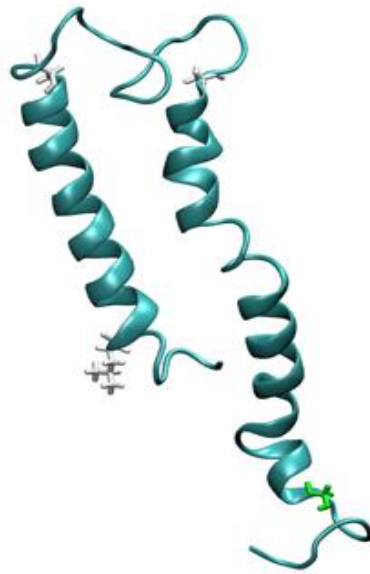


Figure 1. COR15A structure based on molecular dynamics simulations in vacuum. This figure shows the in vacuum structure of COR15A based on molecular dynamics simulations, and highlights the residues flanking the helical segments of COR15A. The structures in white are the non-polar residues and the green structure represents a polar molecule.

Previous experiments by our collaborators and other researchers have shown that COR15A preserves the activity of lactate dehydrogenase (LDH) using freeze thaw experiments [19]. Though COR15A has been shown to stabilize LDH, there is no evidence to suggest that it is involved in the stabilization of chloroplast localized enzymes under dehydrating conditions, but it has been shown to stabilize membranes [19, 27]. COR15A has been shown to interact with chloroplast membrane lipids such as monogalactosyldiacylglycerol (MDGD) and digalactosyldiacylglycerol (DGDG) [19]. Previously performed experiments in the field established that overexpression of the chloroplast protein COR15A in plants increases tolerance of plant leaves to cold temperatures by decreasing the temperature at which damage occurs [26, 28]. To stabilize membranes and increase freezing tolerance under dehydrating conditions, the proposed mode of action of COR15A is to bind to membranes and stabilize the lamellar phase.

This in turn will decrease the incidence of the structural phase transition from lamellar to hexagonal phase II (Figure 2A&B) [27].

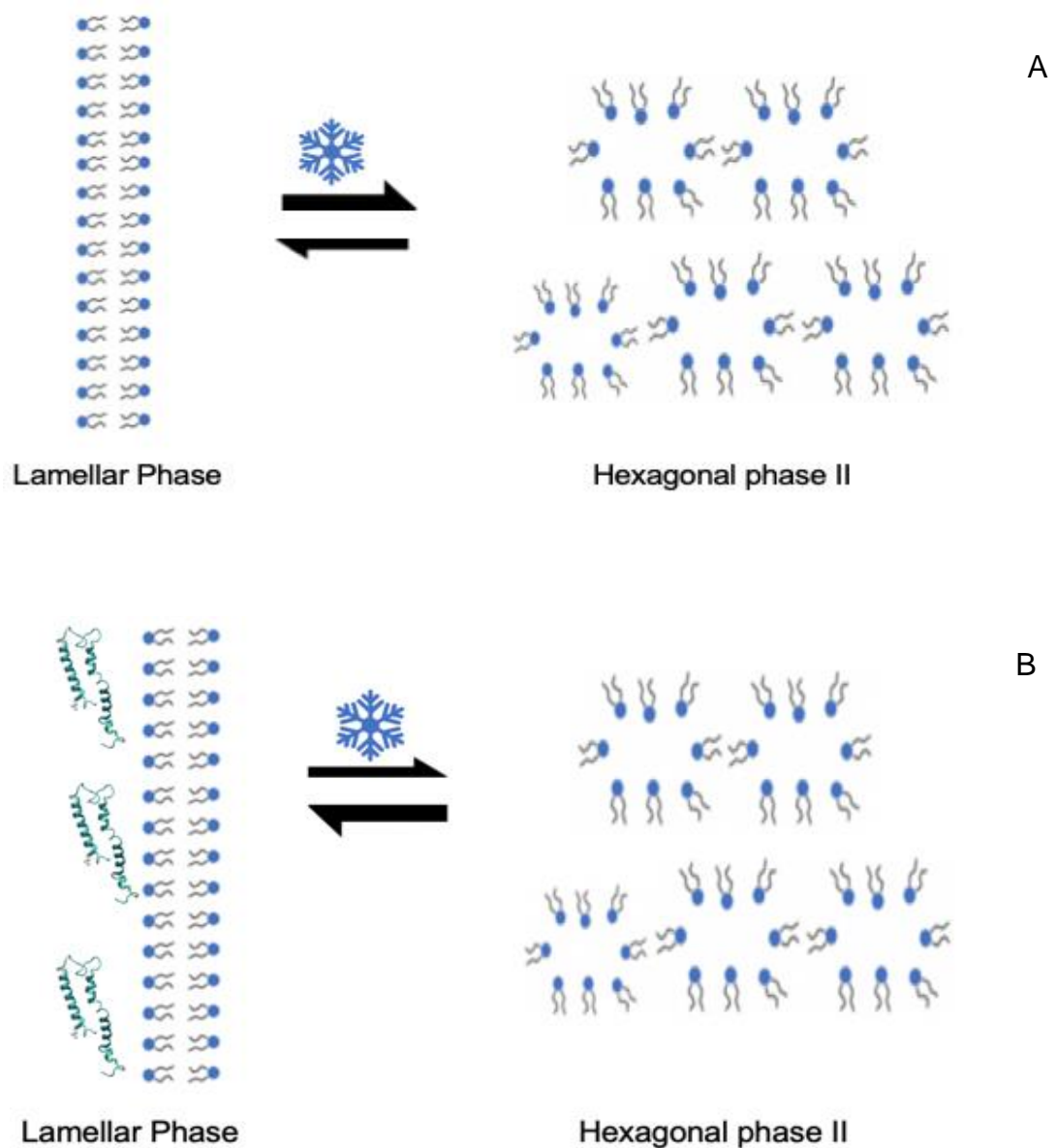


Figure 2. Change in membrane lipid structure due to freezing conditions in the absence and presence of COR15A. A: In the absence of COR15A, the membrane lipids in the plant's chloroplast undergo a lamellar to hexagonal phase II transition under freezing conditions. B: In the presence of COR15A, the lipids are stabilized, and this reduces the temperature at which the phase transition from lamellar to hexagonal phase II occurs.

1.4 Specific Aims

Cold regulated protein COR15A is a nuclear-encoded intrinsically disordered protein found in plants such as *Arabidopsis thaliana*. It is responsible for increased tolerance in plants when expressed under cold induced dehydrating conditions. The proposed mechanism for COR15A involves an increase in its α -helical content and stabilization of the chloroplast membranes by interacting with the chloroplast membrane lipids. The structural transition of COR15A under dehydrating conditions is proposed to be essential for its function. This led to our hypothesis that mutations in the amino acid structure of specific residues in COR15A can lead to an increase in its helical content, which also leads to an increase in its protective function. In order to test our hypothesis, we examined the structure of COR15A to determine which amino acid residues are important for maintaining its disordered structure, what happens to the structure of COR15A when these residues are mutated, and how these mutations affect the function of COR15A. Our hypothesis was tested using the aims described below.

Aim 1 (Chapter 2): Determine the amino acid residues that are important for maintaining the structure of COR15A, and how the structure of COR15A is affected when they are mutated.

Aim 2 (Chapter 3): Determine the effect of increased helical content on the function of COR15A.

CHAPTER 2

Identification and analysis of the amino acid residues that maintain the disordered structure of COR15A

Note to readers: This chapter contains information, including figures, published in *Biomolecules* 2019, 9(3), 84, and permission has been granted for this reproduction.

2.1 Rationale: Conservation of key amino acid residues in COR15A's amino acid sequence.

The presence of certain types of amino acids in IDPs prevent the formation of secondary structure, hereby stabilizing the disordered structure of the protein [4, 8, 10]. It is hypothesized that COR15A is disordered in its hydrated state, but when the plant is exposed to cold induced dehydration it undergoes a structural transition that makes it more helical in structure [27]. This disorder to order transition is suggested to influence its ability to stabilize the chloroplast membrane because it is only in its helical state that it is proposed to interact with and stabilize chloroplast membranes [19, 27, 29]. To determine which residues are important for maintaining the disordered structure of COR15A, we performed sequence alignments on COR15A homologues from different plant species (**Figure 3**). The sequences used in the alignment were obtained from a BLAST search using the nonredundant sequence database and aligned using Geneious. Predictions of the % helical content of the homologs was also performed using AGADIR (**Table 1**), and of the 6 homologs only *Triticum aestivum* had a helical content that was higher than that of WT COR15A from *Arabidopsis thaliana*. From the sequence alignments

(Figure 3), it can be seen that there are four glycine residues conserved across all seven homologs, while the COR15A sequence has seven glycine residues in total. The presence of the glycine residues is important because, as mentioned previously, glycine residues in IDPs impede the formation of secondary structure [8, 10]. Based on the sequence alignments, we also observed a great number of salt bridges in the *Arabidopsis thaliana* sequence. Previous research by the Thalhammer group has shown that dehydration stabilizes salt bridges [26]. The charged residues in the *Arabidopsis thaliana* sequence that are not involved in the formation of salt bridges are K4, D6, E44, E80 and K87. Amino acid residues i-4 and i+4 from these residues were then substituted for alanine residues, and charged residues, but none of these mutants were predicted to increase the helical content of COR15A as much as the G68A mutation based on AGADIR predictions (Table 2). Based on the alignment, we decided to test how mutations of some of the glycine residues to alanines will affect the structure of COR15A.

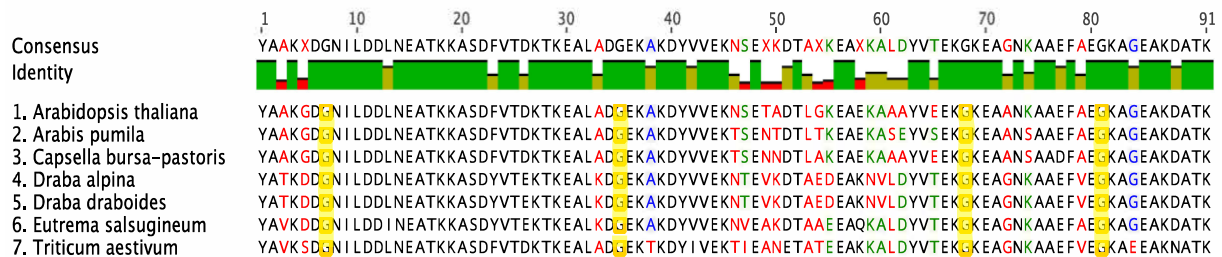


Figure 3. Sequence alignment of COR15A homologs in various plant species. The structure of COR15A from various plant species was analyzed using sequence alignments. In this sequence alignment, the black letters indicate 100% sequence similarity, the blue letters indicate 80% - 99%, the green letters indicate 60% - 79%, and the red letters indicate less than 60% similarity. The residues highlighted are the glycine residues that are conserved in the examined homologs.

2.2 Effects of conserved glycine residues on the structure of COR15A.

To test the effect of the glycine residues on the structure of COR15A, AGADIR predictions of %helicity and IUPRED predictions of disorder were performed. Each of the glycine residues were substituted one at a time to determine which single mutant will be made and tested using NMR experiments Figure 4. Then multiple substitutions of the glycine residues were then

performed to determine which combination of multiple glycine mutations will increase the α -helical content of COR15A the most **Figure 5**.

Table 1. % Helix prediction of COR15A in *Arabidopsis thaliana* and its homologs. This table shows the AGADIR predicted α -helical content of COR15A from *Arabidopsis thaliana*, and its homologs from figure 3 above.

COR15A Homolog	AGADIR % Helix
<i>Arabidopsis thaliana</i>	3.97
<i>Arabis pumila</i>	3.27
<i>Capsella bursa-pastoris</i>	3.89
<i>Draba alpina</i>	3.22
<i>Draba draboides</i>	3.22
<i>Eutrema salsugineum</i>	3.82
<i>Triticum aestivum</i>	4.95

Table 2. AGADIR % helix prediction of residues downstream and upstream from charged residues not involved in salt bridge formation. This table shows the % helix predictions for residues i-4 and i+4 from charged residues not involved in salt bridge formation in the *Arabidopsis thaliana* protein sequence.

COR15A mutation	AGADIR % Helix
WT	3.97
G68A	6.08
4GtoA	7.51
N8A	3.97
N8K	3.98
N8E	3.97
A2K	3.97
A2E	3.97
L10K	3.97
L10E	4
L10A	3.97
A76K	4.12
A76E	3.67
A83K	4.02
A83E	3.93
K91A	3.97
K91E	3.97

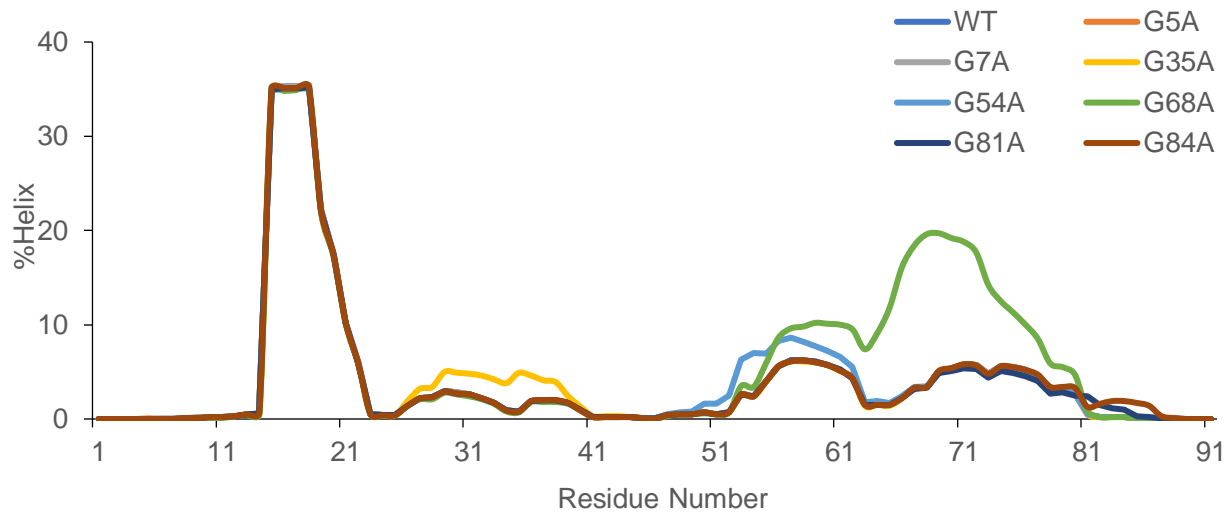


Figure 4. AGADIR %Helix predictions for COR15AWT and single alanine substitutions. The %Helix predictions for COR15AWT and the individual glycine to alanine substitutions was plotted against the residue number. This graph shows the predicted helical regions in these protein sequences.

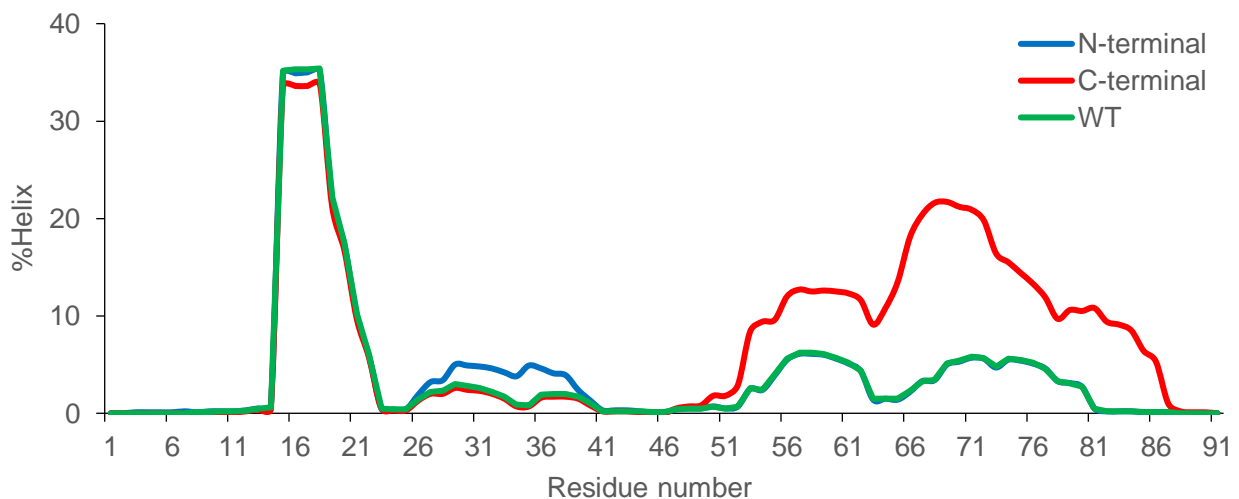


Figure 5. AGADIR %Helix predictions for CORWT and N- and C- terminal mutants. The green line represents COR1A WT. The blue line which represents the N-terminal represents the %helix prediction for COR15A when glycine residues 5,7 and 35 are mutated to alanine. The red line represents wt, and this shows the %helix prediction when glycine residues 54,68,81, and 84 are mutated to alanine.

In **figure 4** , it can be seen that COR15A G68A has the highest predicted % helix according to AGADIR. AGADIR predicts that the G68A mutation in COR15A will increase the helical content

of COR15A from 3.97% in WT to 6.08%. In **figure 5**, the AGADIR predictions indicate that mutating the N- terminal glycine residues to alanine will increase the α -helical content of COR15A from 3.97% in WT to 4.25%, while mutating the C-terminal glycine residues will increase the α -helical content to 7.51%.

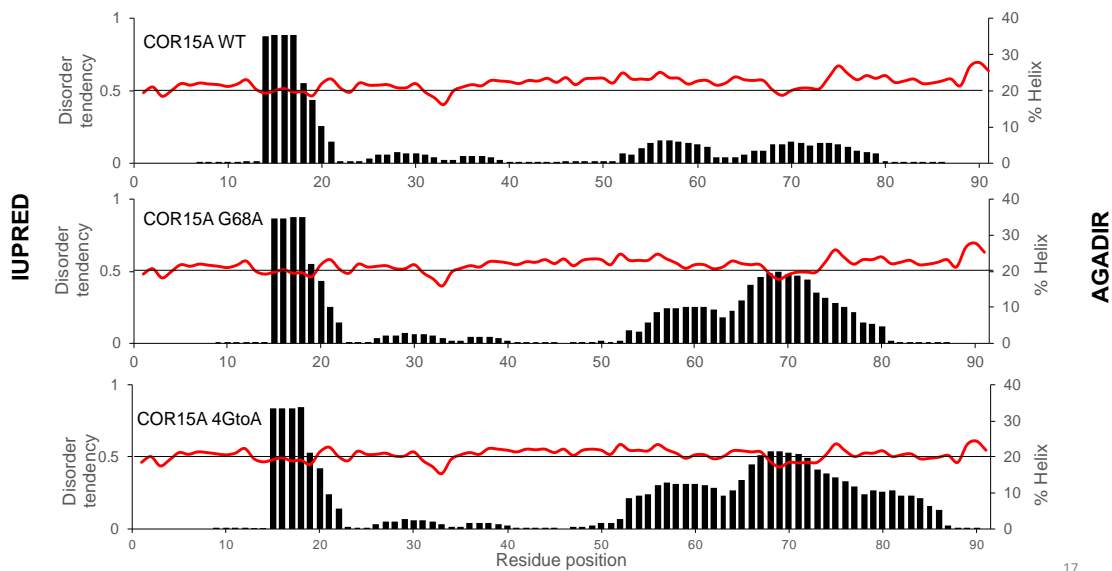


Figure 6. AGADIR %helix and IUPRED disorder predictions for individual residues in COR15A WT and mutants. The AGADIR predictions are represented by the black bars, while the IUPRED predictions are represented by the red line. A: COR15A WT. B: single mutant G68A, C: quadruple mutant 4GtoA. The primary vertical axis represents disorder tendency as predicted by IUPRED, while the secondary vertical axis depicts the %helix as predicted by AGADIR. The horizontal axis represents the residue number/position.

Based on these predictions the single mutant selected was COR15A G68A, and the quadruple mutant chosen was the one with the glycine residues at the c-terminal mutated to alanine **Figure 5**. **Figure 6** shows the overlay of the AGADIR % helix predictions and the IUPRED disorder predictions for CORWT and the selected mutants. All the AGADIR predictions (**Figures 4-6**) show that there are two helical segments in all the COR15A sequences examined. In **Figure 6 A-C** it can be seen that the % helix predicted for the N-terminus is about the same in COR15A WT and the chosen mutants. In the N-terminal helix, the average α -helicity for residues 15-22 is 24%. For the C-terminal helix, the % helical content for residues 53-79 increases from ~4% in WT to 11% in G68A and 14% in the quadruple mutant 4GtoA (**Figure 6 A-C**). For the IUPRED

prediction of disorder, values above 0.5 indicate that the protein is disordered, while values below 0.5 indicate that the protein may be less disordered [30, 31]. The IUPRED disorder prediction for COR15AWT and mutants in **Figure 6 A-C** shows the WT and mutant proteins are borderline in terms of disorder. From WT to G68A to 4GtoA there is a slight shift downward from the 0.5 line, but the difference between the three sequences is not significant.

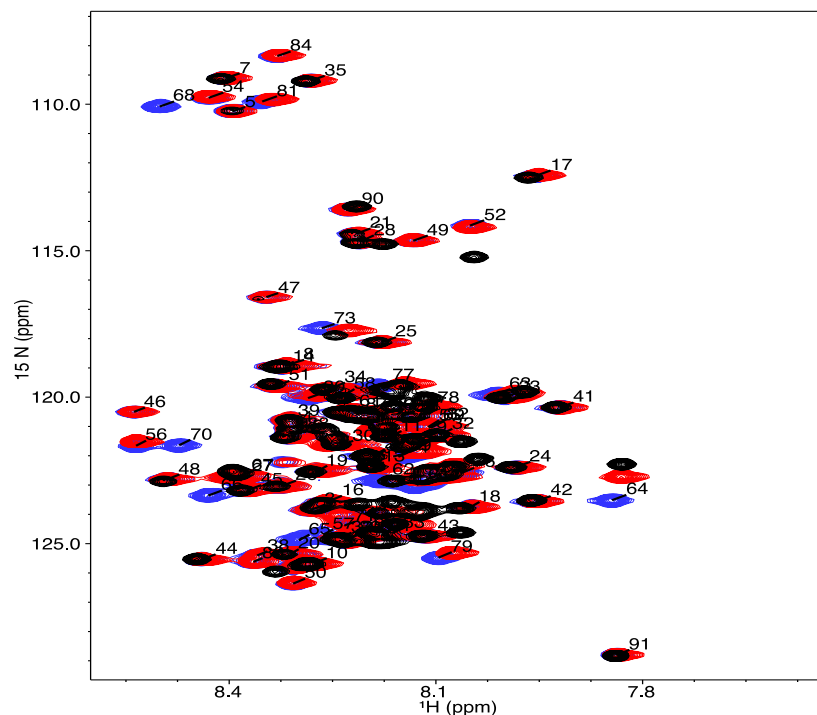


Figure 7. ^1H - ^{15}N HSQC NMR spectra for COR15A WT and mutants in the absence of TFE. The blue peaks depict the WT protein, the red peaks the single mutant G68A and the quadruple 4GtoA mutant is represented by the black peaks. The peaks are labeled with the residue-specific assignments for the WT protein.

The sequence alignments, as well as the results of the AGADIR and IUPRED predictions were the determining factors in choosing the single mutant COR15A G68A and the quadruple mutant with glycine residues 54,68,81 and 84 mutated to alanine. The next step was to perform NMR experiments on the WT and the mutants, to compare the difference in helical content as a result of the point mutations. The first NMR experiment performed on the WT and mutant proteins was ^1H - ^{15}N heteronuclear single quantum coherence (HSQC) (**Figure 7**). The overlaid spectra of all three proteins shows the amino acid dependent secondary chemical shift of all 91 residues.

The distribution of these chemical shifts (**Figure 7**), does not indicate any significant structural changes, and the ^1H - ^{15}N HSQC spectra alone cannot be used for residue specific assignments of the chemical shifts. Therefore, some 3D NMR experiments namely HNCACB, HNCO and CBCACONH were performed. The data from the 2D and 3D NMR experiments were processed using NMRFX Processor, and the residue specific assignments were performed using NMRViewJ (**Figure 8**).

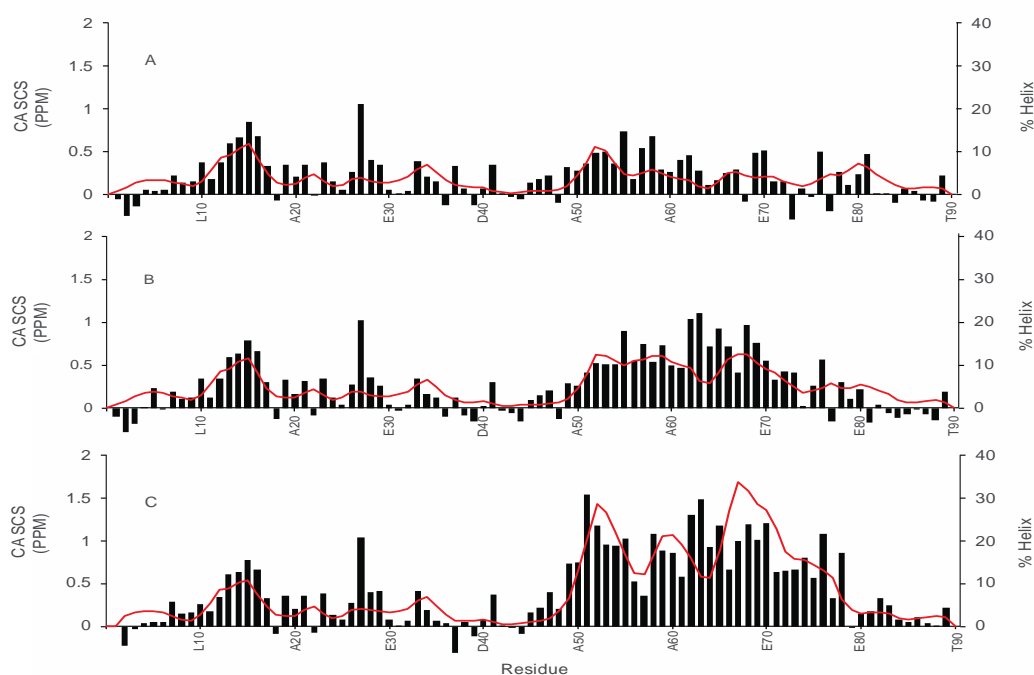


Figure 8. Residue- specific alpha carbon secondary chemical shift and % helix plot for COR15A WT and mutants in 0% TFE. Alpha carbon secondary chemical shifts (black bars) and % helix values (red line) measured using NMR experiments for COR15A WT and mutants in the absence of TFE are shown. The NMR experiments used include ^1H - ^{15}N HSQC, HNCACB and HNCO. The alpha carbon secondary chemical shifts are on the primary vertical axis and the measured % helix values are on the secondary vertical axis, while the residue number/position for every ten residues is on the horizontal axis. A: COR15A WT, B: single mutant G68A, which has the glycine at residue 68 mutated to an alanine, C: quadruple mutant 4GtoA, with glycine residues at positions 54, 68, 81 and 84 mutated to alanine residues.

In **Figure 8 A-C**, the residue specific α -carbon secondary chemical shift and % helix plot of COR15A WT and mutants is shown. This plot was used to compare the α -helical content of all

three proteins as measured and calculated using 2D and 3D NMR experiments. These plots like the AGADIR plots (**Figures 4-6**) also indicate that there are two helical segments in the COR15A protein sequence, and these helical segments are connected in the middle by a segment that acts somewhat like a linker. The plot shows that the N-terminal helix is about the same in the WT and mutant proteins, while the C-terminal segment increases in helical content from the WT via the G68A mutant to the 4GtoA mutant. The average helicity for the N-terminal helix from residue 11-30 is ~4.9% in all three proteins. In the C-terminal segment, the helical content for residues 50-79 increases from 4.4% in WT to 8.5% in G68A to 18.6% in 4GtoA. The helical content for the N-terminal segment of WT COR15A measured/calculated using NMR is about a quarter of the % α -helix value predicted by AGADIR. The α -helical content of the full of COR15AWT sequence calculated using NMR is 3.7%, which is similar to that calculated using the Chen algorithm (3.5%), and less than calculated using CDpro using circular dichroism experiments previously performed by the Thalhammer group [26, 32, 33].

2.3 The effect of 20%TFE on the helical content of COR15A WT and Mutants

Following the NMR experiments in **figures 7 & 8** above, NMR experiments were also performed on COR15AWT and mutants in the presence of TFE. As stated earlier, under cold induced dehydrating conditions in *Arabidopsis thaliana*, there is an increase in the helical content of COR15A as it works to protect the plant, by interacting with chloroplast membrane lipids [19, 22, 26]. Trifluoroethanol (TFE) is a co-solvent that stabilizes/induces the formation of α -helices in peptides, and it has been used in NMR experiments [34]. The addition of TFE to COR15A WT and mutants is proposed to mimic the dehydrated state of COR15A under cold induced dehydrating conditions. The effect of TFE on the helical content of COR15A WT and mutants was first examined using ^1H - ^{15}N HSQC NMR experiments (**Figure 9**).

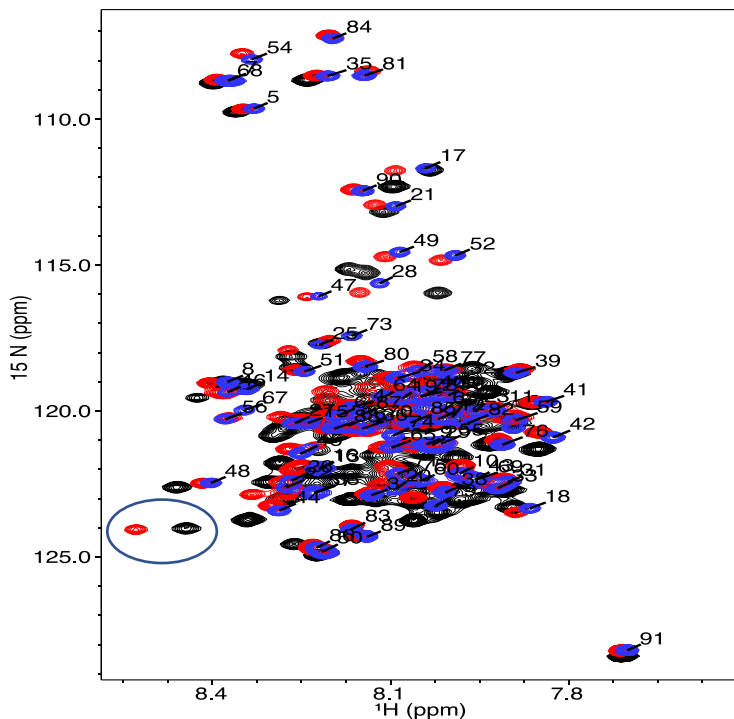


Figure 9. ^1H - ^{15}N HSQC NMR spectra for COR15A WT and mutants in the presence of 20% TFE. The blue peaks depict the WT protein, the red peaks the single mutant G68A and the quadruple 4GtoA mutant is represented by the black peaks. The peaks are labelled with the residue-specific assignments for the WT protein and the two circled unlabeled peaks at the bottom left

The HSQC overlay of COR15A WT and mutants in the presence of TFE shows some slight changes in the backbone chemical shifts, which indicate an increase in helical content (**Figure 9**). These changes are most apparent in the single and quadruple mutant (circled in **Figure 9** above), as the peaks are a bit more dispersed. To further determine the extent of the structural changes, we followed up with some 3D NMR experiments (HNCACB, HNCO and CBCACONH) as we did previously in the absence of TFE (**Figure 10**).

An increase in the helical content of the two helical segments of COR15A is observed in the presence of 20% TFE (**Figure 10 A-C**). Each mutant increased in helical content in 20% TFE, when compared to itself in 0% TFE (**8 A-C**), but the trend of increasing helicity from WT to single mutant to quadruple mutant observed in the 0% TFE sample was not observed in the 20% TFE

samples. The middle region which is proposed to act as a linker, is still relatively disordered compared to the N and C terminal helical regions.

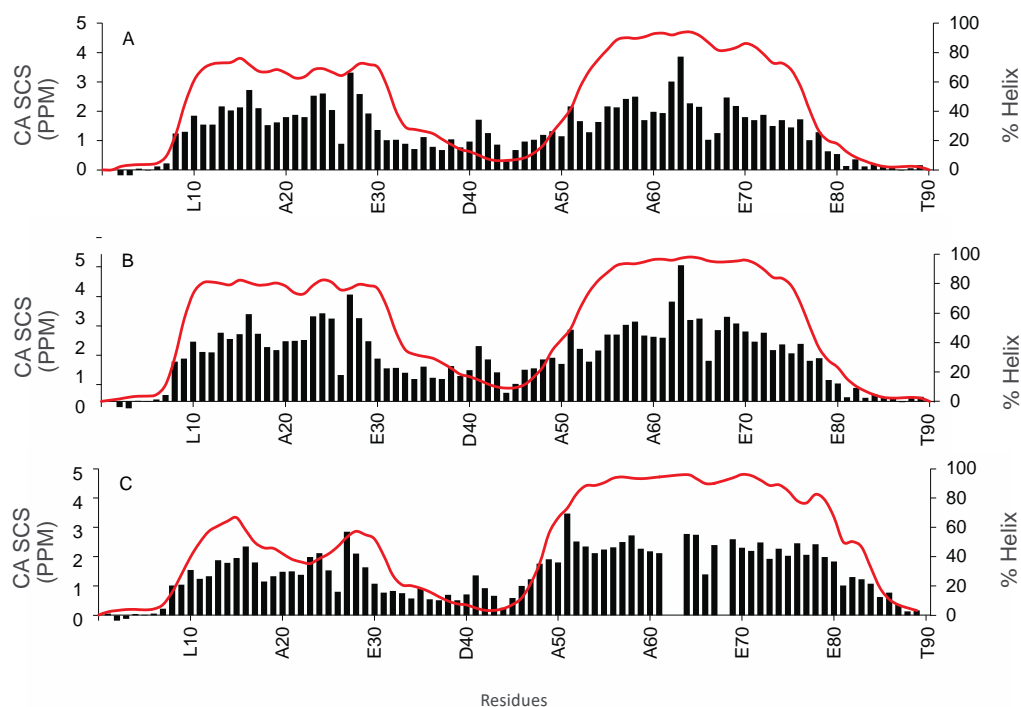


Figure 10. Residue-specific alpha carbon secondary chemical shift and % helix plot for COR15A WT and mutants in the presence of 20% TFE. Alpha-carbon secondary chemical shifts (black bars) and % helix values (red line) measured using δ^{2D} data for COR15A WT and mutants in the presence of 20% TFE. The alpha-carbon secondary chemical shifts are on the primary vertical axis and the measured % helix values are on the secondary vertical axis, while the residue number/position for every ten residues is on the horizontal axis. A: COR15A WT, B: single glycine mutant G68A, C: quadruple mutant 4GtoA, with glycine residues at positions 54, 68, 81 and 84 mutated to alanine residues.

The average α -helical content of the N-terminal residues 11-30 increases from 68.59% in WT (**Figure 10 A**) to 78.7% in the single mutant (**Figure 10B**), then it decreases to 49% in the quadruple mutant (**Figure 10C**). The decrease observed in the helical content is also seen in the α -carbon secondary chemical shift values, where the average WT value is 2 ppm, G68A is 2.3 ppm and 4GtoA is 1.7 ppm, even though there are no mutations in the N-terminal segment (**Figure 10 A-C**). At the c-terminal, residues 50-91, all the proteins have a greater helical content than that N-terminal. The helical content in WT is 74%, in G68A it is 82%, and in 4GtoA it is 87%. This

trend of increasing helical content of the C-terminal helix from WT to the single mutant to the quadruple mutant, was also observed in the 0%TFE samples, but to a lesser extent. The overall α -helical content of COR15AWT observed in 20%TFE for both helical segments is 47.5%, which is similar to that calculated using the Chen algorithm which got 49.7%, and less than that obtained using CDpro which got 56.4%, based on circular dichroism experiments previously performed and published by the Thalhammer group [26, 32, 33]. At the C-terminal residues 50-79, the α -carbon secondary chemical shifts increase from 1.9 in WT to 2.2 in G68A to 2.3 in 4GtoA. The difference in the α -carbon secondary chemical shift values observed here is not as significant as the average difference between the WT and mutants is ~ 0.2 ppm.

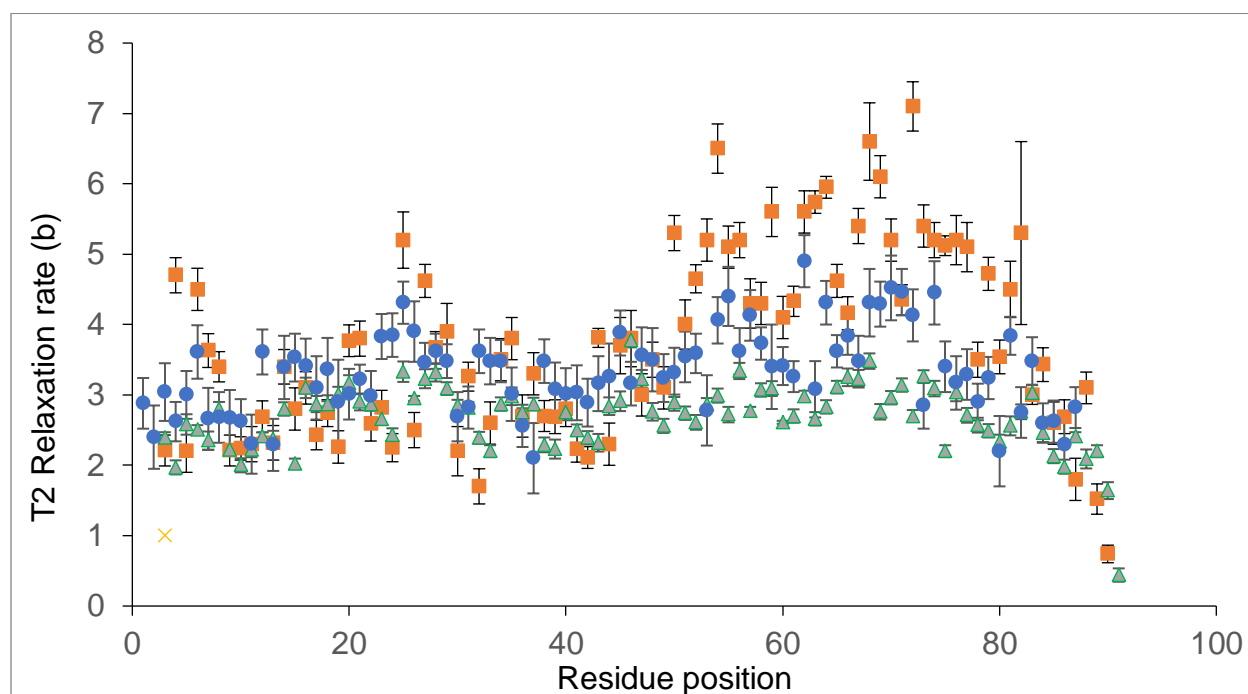


Figure 11. COR15AWT and mutants T2 plot. This plot shows the overlay of the T2 relaxation data for COR15AWT and mutants in 0%TFE. The green triangle represents WT, the blue circle represents G68A and the orange square represents 4GtoA.

Figure 11 above shows the transverse (T2) relaxation for COR15A WT and mutants. T2 relaxation occurs as a result of molecular motion at any frequency, therefore, as molecular reorientation slows down, T2 rates get shorter. In this figure we noticed that at the N-terminal, the relaxation rate for all three proteins is about the same, and this correlates with the α -carbon

secondary chemical shifts/ δ 2D plot in **Figure 8** above, where all three proteins have about the same helical content and α -carbon secondary shifts. At the C-terminus, we notice that the 4GtoA quadruple mutant has the highest T2 values, followed by the G68A single mutant and WT, this also correlates with what we see in **Figure 8** above because 4GtoA has the highest helical content at the c-terminus compared to G68A and WT in 0% TFE. After collecting all the NMR data, we decided to see if indeed the increase in the helical content of COR15A using the glycine to alanine mutants increased the ability of COR15A to stabilize chloroplast membrane lipids. The methods used to test this part of the hypothesis is described in chapter 3 below.

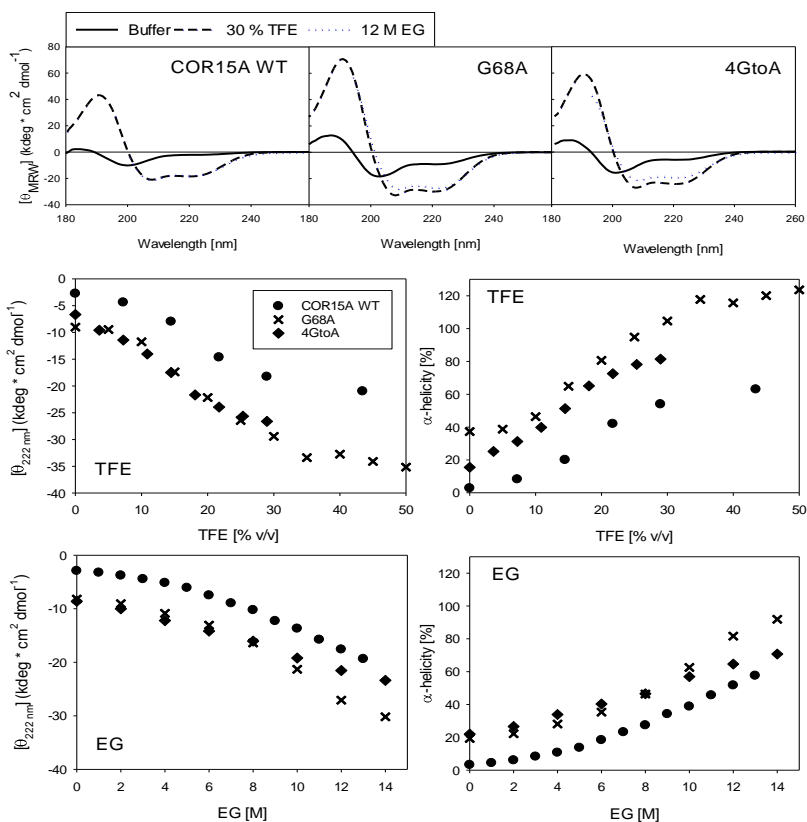


Figure 12. Far-ultraviolet (UV) circular dichroism (CD) spectra in buffer, 20 (v/v) % TFE and 12 M Ethylene Glycol for COR15A WT, G68A and 4GtoA (A). The mutants have more α -helical spectra than the WT in buffer alone, and in the presence of high concentrations of both co-solvents. Coil-helix transitions of COR15A WT and both mutants in TFE (B) and EG (C), specified by θ_{MRW} at 222 nm (left panels) and derived α -helix ratios (right panels).

Far-UV CD spectroscopy was used to investigate secondary structure transitions of COR15A WT and mutants in response to increasing concentrations of the co-solvents TFE and ethylene glycol (EG) (**Figure 12**). Both mutants are more α -helical in low salt phosphate buffer and in high concentrations of TFE, in agreement with the NMR data. The osmolyte EG presents a useful model system for the severely reduced water availability in a cellular environment during freezing, which COR15A encounters under physiological conditions. The concentration range of EG used in our analysis corresponds to osmolarities plant cells encounter in physiological freezing temperatures down to about $-30\text{ }^{\circ}\text{C}$ [35]. Interestingly, all three proteins show comparable CD spectra in 30% TFE and 12 M EG, indicating that a similar coil–helix transition of COR15A and the mutants can be induced by both co-solvents and thus underlining the relevance of the NMR data acquired in TFE. The coil–helix transitions seem to be mostly complete at 30% TFE for COR15A WT and G68A. We were not able to record CD spectra of 4GtoA in sufficiently high TFE concentrations to reach a stable post-transition stage due to protein aggregation, so we cannot state a similar finding for 4GtoA. It is obvious from the CD spectra and the derived α -helicity that the latter must be slightly overrated, which is most likely due to an underestimation of protein concentration. This is a general problem for IDPs due to the underrepresentation of aromatic amino acids [36]. Thus, the α -helix ratios cannot be directly compared to those derived from NMR analyses. However, as all three proteins present an identical molar extinction coefficient at 280 nm, a direct comparison of the ellipticities and the derived α -helicity among the proteins is valid. Both mutants are noticeably more α -helical than the WT in the absence of co-solvent and throughout the complete co-solvent induced transition. As the transitions in most cases lack well-defined pre- and post-transition baselines, the co-solvent concentration in the transition midpoints cannot be determined exactly but only estimated to be similar for all three proteins. Differences between the mutants are obvious. G68A is more α -helical than 4GtoA over the whole range of TFE concentrations and at EG concentrations above 10 M, thus corroborating and strengthening the NMR data in 20% TFE. Interestingly, the α -helicity of 4GtoA and G68A are similar in the

absence of co-solvent. However, upon increasing TFE and EG concentrations, G68A becomes considerably more α -helical than 4GtoA, evidencing a higher overall folding propensity. In contrast, the overall folding propensity of 4GtoA is similar to the WT.

CHAPTER 3

Examining the effect of increased helical content on the function of COR15A.

Note to readers: This chapter contains information, including figures, published in *Biomolecules* 2019, 9(3), 84, and permission has been granted for this reproduction.

3.1 Rationale

Previous research has established that in the hydrated state, COR15A is disordered, but when exposed to freeze induced dehydration, it experiences an increase in helical content [26-28]. The NMR experiments showed that COR15A WT and mutants increased in helical content in 20% TFE compared to 0% TFE. It was also observed that in 20% TFE, the single mutant (G68A) had the highest helical content at the N-terminus. Based on these results and, on our hypothesis, we decided to investigate if the increase in helical content translates into an increase in protective function.

3.2 COR15AWT/MDMX solubility test

We attempted a solubility assay using COR15A WT and MDMX. We chose MDMX because it is an unstable protein that is readily available in our laboratory. MDMX precipitates after a few days when concentrated above 100 μ M, while COR15A can be concentrated to over 4 mM and precipitation is still not observed. The goal of the experiment was to determine if the presence of COR15 in buffered MDMX while it (MDMX) is being concentrated will increase

concentration at which MDMX precipitates. We started with determining the condition under which the experiment will be performed.

In our lab, we work with several fragments of MDMX, so we first had to choose the fragment that will work best. We started with MDMX 23-111, but when we added COR15A to a buffered sample, we could not distinguish the two because their molecular weights are very close. Based on this we decided to use MDMX fragment 23-190. This fragment is quite unstable, and its molecular weight (is higher than that of COR15AWT so they are distinguishable from each other on an SDS-PAGE gel. One parameter we had to figure out is the temperature and time. So, we made buffered mixtures of COR15AWT and MDMX 23-190 with a concentration ratio of COR15AWT : MDMX 23-190 OF 10:1. Though we had decided to use a concentration ratio of 10:1, we still did not know which concentration will work best. So, while we were testing for the best temperature, we were also testing for the best concentration. We had 2 buffered solutions of 200 μ M and 400 μ M concentration of MDMX, and 2 buffered solutions of MDMX 23-190 + COR15AWT. In the first mixture, the concentration of MDMX was 200 μ M and the concentration of COR15AWT was 2 mM. in the second mixture, the concentration of MDMX 23-190 was 400 μ M and the concentration of COR15AWT was 4 mM. The 4 different samples above were aliquoted into 3x116 μ L each. One aliquot of each sample was placed on the lab bench for room temperature measurements, the other was placed in an incubator at 37°C and the last set was placed in a water bath at 42°C. After these trials, it was determined that the best concentration was 400 μ M of MDMX and the best temperature was 42°C. this is because under those conditions we were able to detect precipitation much more quickly. Initially the experiments had a duration of 4 hours, but we saw that some changes were still occurring past 4 hours, so we extended the time to 8 hours. At first, we were looking at the change in concentration of both the pellet and the supernatant as measured using UV absorbance at 280nm, then we settled for just measuring the concentration of the supernatant as the results were somewhat more consistent.

Most of the steps described above changed as the experiment evolved, but the working procedure for the solubility test is below.

Solubility test steps

- 1) After COR15AWT and MDMX 23-190 were purified, they were both dialyzed into low salt phosphate buffer (recipe is after the procedure) with DTT due to the cystine residues in MDMX.
- 2) Concentrate 200 μ l of MDMX alone at 200 μ M to 400 μ M (100 μ L)
- 3) Concentrate 200 μ l of MDMX at 200 μ M + 200 μ l of COR15AWT at 2mM to about 100 μ l.
- 4) Aliquot the MDMX alone samples from step 2 above into 8 Eppendorf tubes
- 5) Aliquot the mixture from step 3 above into 8 Eppendorf tubes (10 μ l each)
- 6) Place the sample from step 5 & 6 above in a water bath at 42°C.
- 7) Take out a sample every hour, spin the sample down, separate the supernatant from the pellet
- 8) Wash the pellet from step 7 above with fresh buffer to get rid of residual supernatant.
- 9) After step 8, spin down the sample and separate the wash buffer from the pellet
- 10) Place the samples from step 8 in a speedvac to dry out the pellet
- 11) After drying the pellet, resuspended them in fresh buffer with 6M urea added
- 12) After the pellets are resuspended, run them on a polyacrylamide gel
- 13) Run the supernatant samples from step 7 on a polyacrylamide gel
- 14) Preserve the gels from steps 12 and 13 in a solution containing 5% glycerol and 20% ethanol
- 15) Analyze the protein bands on the gels from step 14 using a densitometer

16) Plot the relative quantity values of the protein band from above to compare the rate of precipitation of MDMX in the absence and presence of COR15A WT

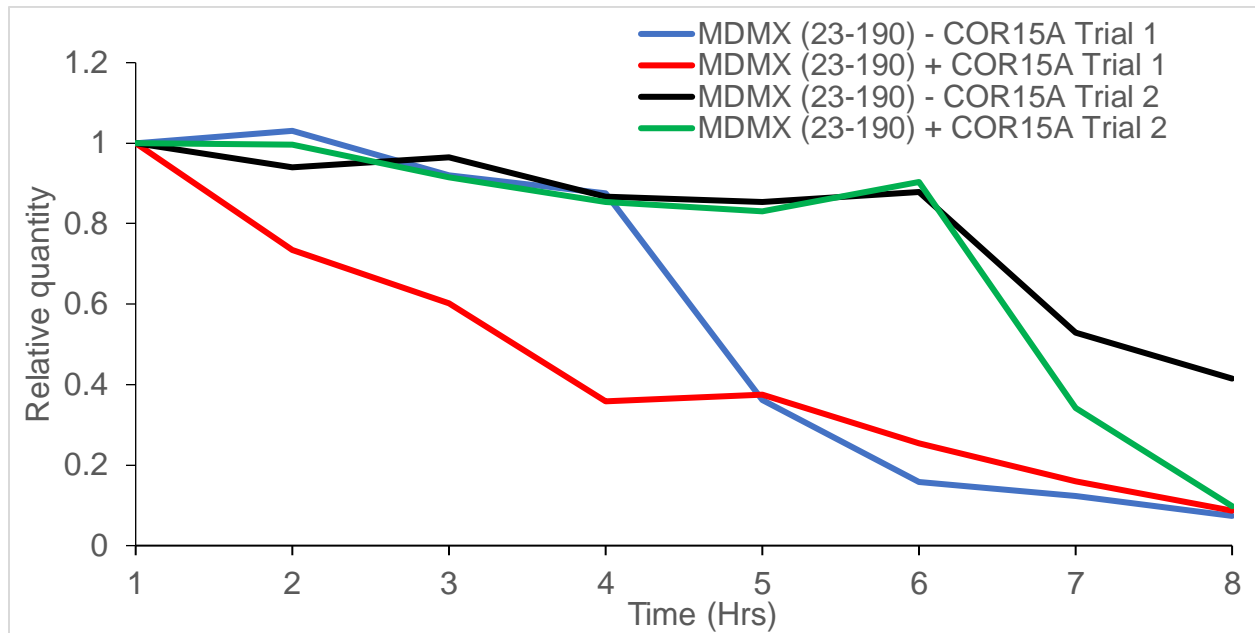


Figure 13. Solubility test plot for the supernatant samples. This plot represents two replicates of the experiment. It shows the decrease in concentration of the supernatant over period of 8 hours due to precipitation.

Figure 13 above shows the change in concentration of the supernatant sample of the MDMX alone and the MDMX + COR15AWT supernatant samples over an 8hr period. The plots show the same experimental conditions repeated twice for the MDMX alone and MDMX + COR15AWT samples. The other run throughs of the experiment were not included because they were mostly inconsistent. If the experiment had yielded consistent results for most of the run throughs, the goal was to try the same protocol with the single (G68A) and quadruple (4GtoA) mutants to see if they decreased the precipitation of MDMX in better than the WT sample.

3.3 Carboxy Fluorescein assay

Previous research has indicated that the interaction of COR15A with galactolipids of inner chloroplast membranes may be the mechanism by which COR15A increases Arabidopsis

freezing tolerance [27]. To test the effectiveness of the COR15A mutants compared to the WT protein in stabilizing these membranes during a freeze-thaw cycle, leakage of the fluorescent dye carboxy fluorescein from LUVs mimicking the lipid composition of these membranes was measured in the presence and absence of recombinant proteins in different protein: lipid molar ratios.

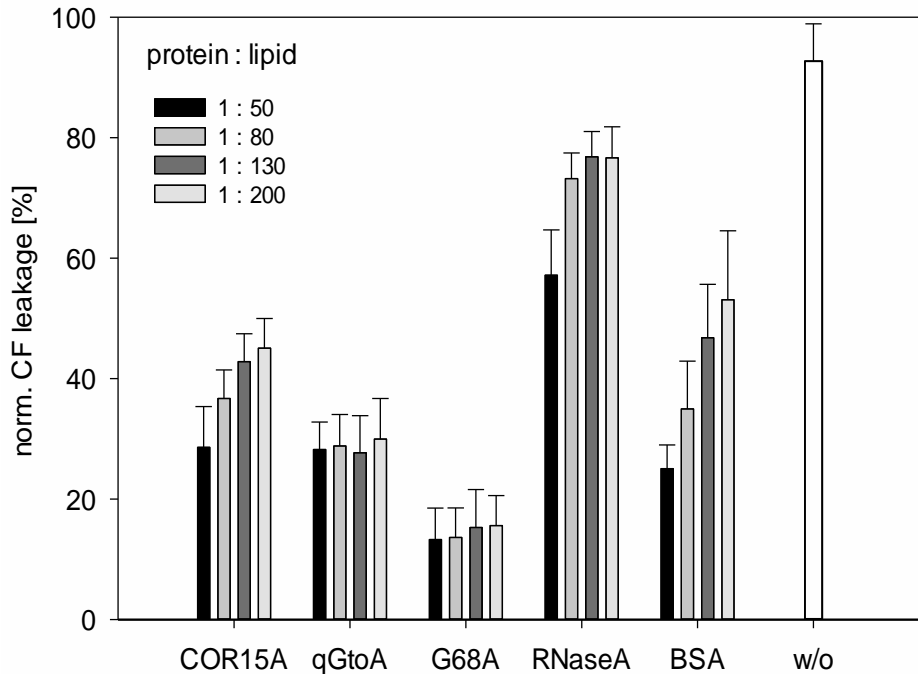


Figure 14. α -helical mutants reduce carboxy fluorescein (CF) leakage from vesicles. Carboxy fluorescein leakage of inner chloroplast membranes (ICMM) large unilamellar vesicles (LUVs) after freezing and subsequent thawing was performed using the fluorescence signal detected by $\lambda_{ex} = 492\text{nm}$ and $\lambda_{em} = 517\text{nm}$. The protein:lipid molar ratios used were 1:50, 1:80, 1:130, 1:200,

Liposomes without any protein added were strongly compromised after freezing and subsequent thawing (**Figure 14**), with dye leakage of about 90%, which is directly proportional to LUV damage. Similar to previously reported results, COR15A WT significantly stabilized the LUVs in a concentration-dependent manner during a freeze–thaw cycle, with dye leakage between 30–50% [37]. The degree of liposome damage in the presence of the two mutants is less than in the

presence of the WT protein. The quadruple mutant 4GtoA showed a small but still significantly better LUV stabilization than COR15A WT ($p < 0.001$) in protein:lipid molar ratios above 1:50. G68A stabilized the LUVs significantly better ($p < 0.001$) than COR15A WT in all tested protein:lipid ratios. This is an interesting finding when combined with the higher overall α -helicity of G68A compared to 4GtoA in high co-solvent concentrations, assuming that COR15A associates with and consequently stabilizes membranes in a folded state as induced by the investigated co-solvents. This finding supports the hypothesis that actually COR15A functionality is directly related to α -helicity. Previous reports suggested that COR15A might form oligomeric structures in the fully hydrated state, as shown by crosslinking experiments [37]. If it actually does so under conditions of reduced water availability, as experienced during freezing, has not been investigated. Thus, we cannot rule out the possibility that COR15A oligomer formation might be impacted in the mutants, thus influencing functionality. In contrast to COR15A WT, the protective effect of the mutants was independent of the lipid:protein ratio, indicating that a lower amount of mutant protein is sufficient to tap their stabilization potential. The reference protein RNase A had a minor, nevertheless significant protective effect on liposome stability, whereas Bovine serum albumin, as a known membrane stabilizer, significantly better protected the LUVs from dye leakage in a concentration dependent manner, compared to COR15A WT. These data corroborate the previous finding of COR15A associating with membranes exclusively in a folded state [24, 38]. The folding state seemingly does not only influence membrane association but consequently also membrane stabilization. So, what is the apparent advantage of COR15A in being intrinsically disordered? The coil-helix transition of COR15A is strictly modulated by the osmolarity of the cellular environment, which increases with decreasing freezing temperature [35]. The major finding we report here is that increased α -helicity of COR15A directly translates into increased functionality. This presents crucial progress in understanding the structure–function relationship of COR15A specifically and should be investigated regarding other LEA proteins in

the future with respect to the long-term perspective of manufacturing plants with improved desiccation, dehydration or freezing tolerance.

CHAPTER 4

DISCUSSION

Note to readers: This chapter contains information, including figures, published in *Biomolecules* 2019, 9(3), 84, and permission has been granted for this reproduction.

4.1 The effect of glycine residues on the α -helical content of COR15A

The importance of conserved glycine residues on maintaining the disordered structure of COR15A using sequence alignments was elucidated first by using the sequence alignments. The sequence alignments in **Figure 3** show that glycine residues at positions 7, 35, 68, and 81 in the COR15A sequence are conserved across several plant species. In addition, the glycine residue at position 84 is mostly conserved and that at position 54 is not. AGADIR predicted that the glycine residue at position 68 had a stronger impact on COR15A disorder than the remaining glycine residues. It also predicted that the glycine residues at positions 54, 68, 81 and 84 in the C-terminal segment of the protein had a stronger impact on the preservation of COR15A disorder compared to the glycine residues in the N-terminal segment. Based on these indications, we made a single glycine to alanine mutation at position 68 and a quadruple mutant at residues 54, 68, 81 and 84. The mutant proteins and COR15A were subject to a detailed structural and functional analysis, and the results showed that the conserved glycines were indeed important in the maintenance of disorder in COR15A. **Figure 15** is a model that shows what we propose happens to the equilibrium between the lamellar and hexagonal phase II structures of the lipids in a chloroplast membrane in response to changing the equilibrium between disordered and helical COR15A.

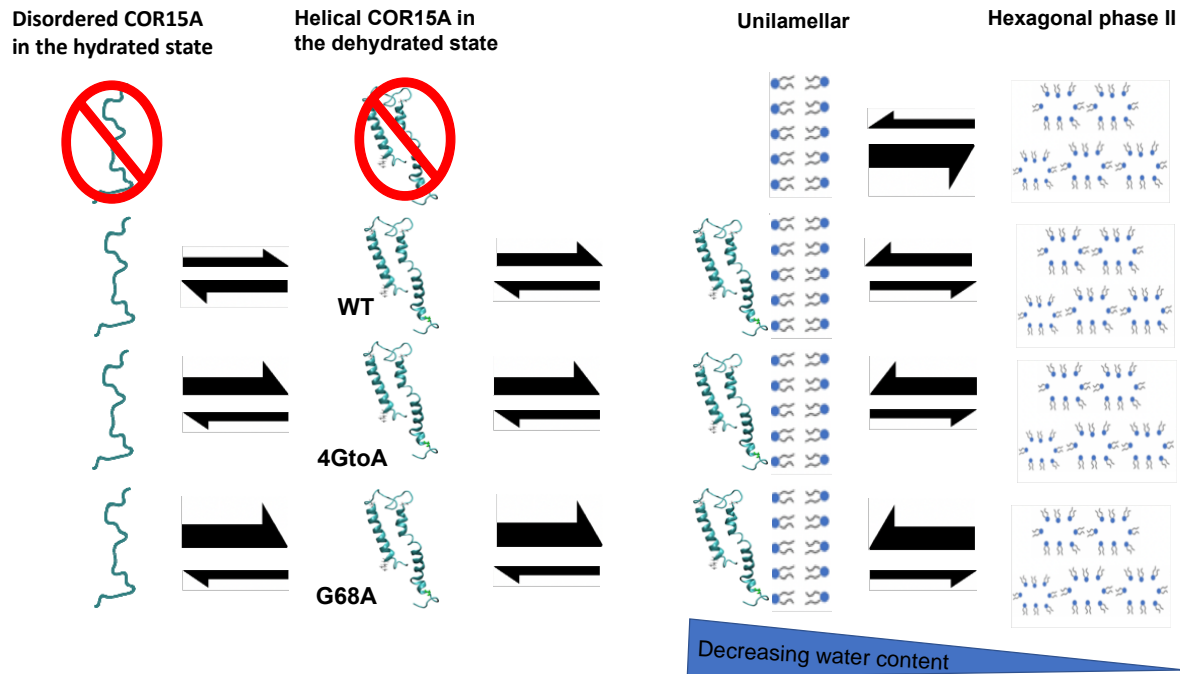


Figure 15. COR15A mutants have a higher helical content and are more protective than COR15A WT. This model summarizes the results of our structural (NMR) experiments and functional (liposome stability) assay. As water content decreases, in the absence of COR15A, the equilibrium favors the formation of the hexagonal phase II structure and not the lamellar structure. In the presence of COR15A under the same conditions, the lamellar phase is increasingly favored going from WT to the G68A mutant. In the 4GtoA mutant, the lamellar phase is still favored compared to wildtype, but not as much as in the G6A mutant.

The first row in **Figure 15** shows that in the absence of COR15A, the equilibrium favors the hexagonal phase II state as the water content decreases. Rows 2 through 4 show our model for disordered and helical COR15A in equilibrium. The size of the arrows is qualitative and relative to the amount of correctly folded COR15A we think is present based on how helical the mutants are compared to WT. It is also based on how well G68A and 4GtoA performed in the liposome stabilization assay and this is reflected on the right side of the figure where we estimate the effects of the more helical mutants on the equilibrium between the lamellar phase and hexagonal phase II. The extent to which each protein tips the equilibrium toward the helical state is correlated with the membrane stability of the large unilamellar vesicles, as shown in **Figure 14**.

The model for the helical state of COR15A shown in Figure 15 is from previous work by Thalhammer and colleagues. They generated a homology model for the dehydrated state of COR15A. In this model, COR15A forms a structure with N- and C-terminal helices separated by a long loop [26]. The length and flexibility of the long loop may control interactions between the N- and C-terminal helix. The position of the helices in the homology model overlaps with the helical segments we identified using NMR. We think the decreasing helicity for the N-terminal helix in 4GtoA compared to G68A is interesting and may support the homology model of COR15A proposed by Thalhammer and colleagues (see below). In 0% TFE (**Figure 8 A–C**), the N-terminal helix (residues 10–31) has an average helicity of 4.6% and is not affected by C-terminal mutations. However, the helicity of the C-terminal helix (residues 50–84) increases from WT (4.6%) to G68A (7.9%) to 4GtoA (16.4%). The 20% TFE samples, show a different trend. The helical content of the N-terminal helix increases from WT (67.6%) to G68A (77.6%), but in 4GtoA (48.1%), the helical content decreases. However, in the C-terminal helix, there is an increase in helical content from WT (65.2%) to G68A (72.3%) to 4GtoA (81.6%). Based on this analysis, we think it is possible that the observed decrease in the helical content of 4GtoA in 20% TFE, may be due to a decrease in the interaction of the two helical segments in 20% TFE due to the G54A mutation. We also think this is why G68A is better at stabilizing the liposomes than 4GtoA.

4.2 Effects of the Glycine to alanine mutations on the function of COR15A

In the solubility test, the goal was to explore the ability of COR15A to stabilize proteins, so we chose a readily available unstable protein MDMX that we had in the lab. MDMX precipitates after a few days if it is concentrated beyond 100 μ M, so we were trying to determine if the addition of COR15A to the mixture will reduce the precipitation of MDMX at high concentration. This experiment seemed quite inconclusive because we could not get consistent results, and the results we got were not significant enough to come to a solid conclusion on what was happening

to MDMX in the presence of COR15A. In some of the reactions, it seemed like COR15A increased the rate of precipitation of MDMX, while in some of them it seemed to decrease this rate.

The NMR and CD studies performed on the WT and mutant proteins showed that in the absence of TFE, COR15A WT had lower α -helicity compared to both mutants. As expected, in the presence of the α -helix-inducing agent TFE, α -helicity was increased in all proteins. While both mutants had higher α -helicity than the WT, the single mutant had higher α -helicity than the quadruple mutant in the N-terminal α -helix. Functionally, higher α -helicity resulted in increased liposome stabilization in response to freezing (**Figure 14**). This effect was greater for the G68A mutant, which showed the highest overall α -helical content in high TFE and EG concentrations. This finding is consistent with our current understanding of membrane association of COR15A via α -helical segments [19, 25, 26]. In our liposome stabilization assay, we tested the ability of the WT and mutant COR15A samples to stabilize chloroplast lipids using unilamellar vesicles that contained the major lipids in the chloroplast of *Arabidopsis thaliana*. The results showed that of the 3 proteins, the G68A mutant was most effective in protecting the unilamellar vesicles from leakage after freeze/thaw cycle. The 4GtoA mutant was better in preventing leakage than the WT protein but not as good as the single mutant G68A. The reduced function of 4GtoA compared to G68A may be due to the G54A mutation. In the COR15AWT and mutant samples as seen in the NMR experiments (**Figure 8 and 10**), the middle region separating the two helices is disordered in the absence and presence of TFE. This disordered region is proposed to act as a linker connecting the N and C terminal helices, and the G54A mutation in the 4GtoA mutant makes this region less flexible hereby preventing the interaction of the helices, and thus dampening the protective function of COR15A.

Chapter 5

Materials and Methods

Note to readers: This chapter contains information, including figures, published in *Biomolecules* 2019, 9(3), 84, and permission has been granted for this reproduction.

5.1 Preparing COR15A WT and mutant samples

5.1.1 Synthesis and sub-cloning

The COR15A plasmid used was synthesized by GenScript in a pET28a vector. The vector has kanamycin resistance, a T7 promoter, a 6x-histidine tag and a thrombin cleavage site. The COR15A gene was inserted in the multiple cloning site downstream from the T7 promoter.

5.1.2 Transformations

The COR15A plasmid (**Figure 16**) was transformed into competent *E.coli* BL21 (DE3) cells which contain the T7 polymerase gene controlled by lacUV5 promoter. Isopropyl β -d-1-thiogalactopyranoside (IPTG) can be used to induce the T7 polymerase. The induction of the T7 polymerase by IPTG leads to expression of the genes in the multiple cloning site. The protocol for the transformation is below.

1. Add 2 μ l of 1ng/ μ l COR15A plasmid to a centrifuge tube containing 20 μ l of BL21 (DE3) cells and gently pipet up and down to mix.
2. Incubate the mixtures from step1 on ice for 10 minutes.
3. Heat shock the mixture in a water bath at 42°C for 30 seconds.

4. Incubate on ice for 2 minutes.
5. Add 125 μ l of SOC rescue media and incubate in a shaking incubator for 1 hour at 37°C and 225 RPM.
6. Plate 100 μ l of the mixture on agar plates containing kanamycin and incubate them at 37°C overnight.
7. A negative control should be made simultaneously. The negative control should be treated like the main sample, and the only difference should be the absence of plasmid.
8. Store the agar plates in the refrigerator (4°C) until they are ready to be used.

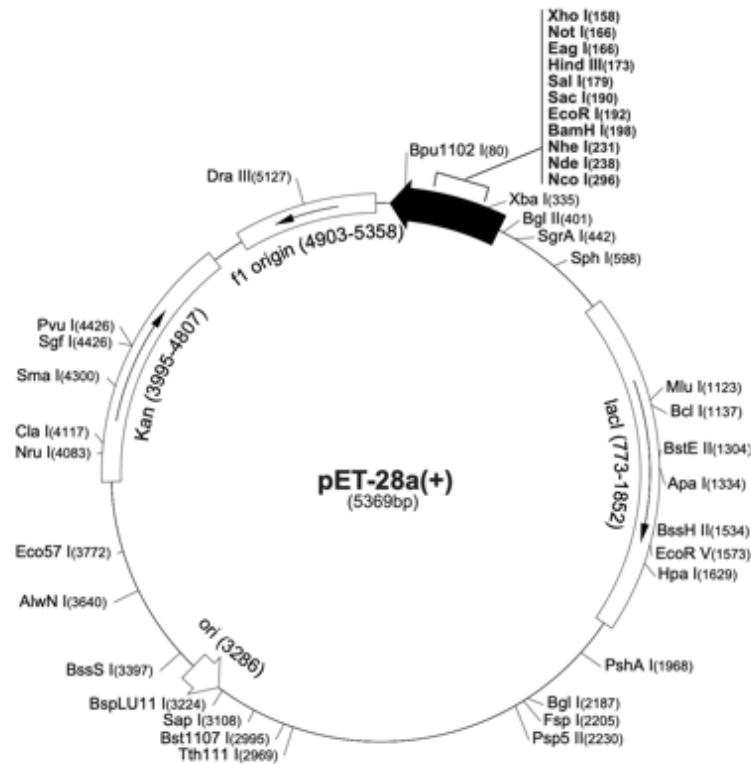


Figure 16. This pET28a vector map showing the locations of the major components. COR15AWT was inserted between BPU1102 and NDE1.

5.1.3 Site directed mutagenesis

The COR15A G68A mutation was obtained by performing site-directed mutagenesis on WT using the Stratagene QuickChange kit. For the mutagenesis, supercoiled dsDNA and forward and reverse oligonucleotide primers containing the mutation were used. PCR was used to extend primers complementary to the opposite strand. The primers used were designed using PrimerX and purchased from Operon. The protocol used is itemized below.

5.1.3.1 Polymerase chain reaction (PCR) set up

1. Mix each primer with Tris elution buffer to bring the final concentration to 100 μ M.
2. Dilute the primer stocks from step 1 to 125ng/ μ l in 50 μ l.
3. Make a 75 μ l master mix by adding
 - i. 7.5 μ l of 10x reaction buffer
 - ii. 3 μ l of forward primer
 - iii. 3 μ l of reverse primer
 - iv. 3 μ l of DNTP mix
 - v. 49.5 μ l of water
4. Aliquot the contents of the master mix into 3 PCR tubes.
5. Make the samples and the control
 - i. To PCR tube 1 from step 4 add 1 μ l of polymerase.
 - ii. To PCR tube 1 from step 4 add 2 μ l of 5ng/ μ l template and 1 μ l of polymerase.
 - iii. To PCR tube 1 from step 4 add 0.2 μ l of 5ng/ μ l template and 1 μ l of polymerase.

5.1.3.2 Polymerase chain reaction (PCR)

The template DNA with the target site for the mutation is denatured and annealed with the primers containing the mutation needed. The thermocycler set up is shown in **Table 3**.

Table 3. Polymerase chain reaction steps as programmed into thermocycler. This table shows the temperature, duration and number of cycles for each step in the PCR process for site directed mutagenesis.

Step	Temperature (°C)	Duration	# of cycles
First denaturation	95 °C	30 seconds	1
Denaturation	95 °C	30 seconds	25
Annealing	55 °C	30 seconds	
Extension	68 °C	8 minutes	
Last extension	68 °C	1 minute	1
Hold	4 °C	_____	_____

5.1.3.3 DpnI digestion

To get rid of the methylated parental DNA strand, DpnI is added. DpnI digests the parental strand, but not the newly created strand which has the mutation, due to the methylation of the parental strand from the *E.coli* cells. The digestion steps are listed below.

1. After the PCR is done, add 0.5 µl of DpnI to the PCR tubes.
2. Spin down the contents of the tubes.
3. Incubate the samples for 2 hours at 37°C.
4. When the digestion is done, store the sample at 4°C.

5.1.4 Transformation

The nicks in the circular double-stranded DNA from the PCR process are repaired after it has been transformed into XL1-Blue *E.coli* cells. The protocol for the transformation is below.

1. Thaw the cells on ice.
2. In a sterile labeled centrifuge tube, add 50µl of XL1-Blue cells.
3. Add 5 µL of the sample from the DpnI digestion.

4. For the control, there should be a sample without DpnI and a second control that has a different plasmid that has been previously transformed successfully.
5. Incubate all the samples to be transformed on ice for 30 minutes.
6. Heat shock for 30 seconds in a water bath at 42°C.
7. Incubate on ice for 2 minutes
8. Add 500 µl of SOC rescue media
9. Incubate in a shaking incubator at 225 RPM and 37°C for one hour.
10. Get agar plates with kanamycin that have been warmed to 37°C.
11. Plate 100 µl of each control on a different plate
12. Plate 100 µl of the sample containing the DpnI digest product on one plate and 50 µl on another.
13. Incubate all the plates at 37°C overnight.
14. Store the plates at 4°C until they are ready to be used.

5.1.5 Sub-cloning

The 4GtoA mutant was obtained from Invitrogen and sub-cloned into pET28a. To sub-clone the 4GtoA plasmid, NdeI and XhoI restriction sites had to be introduced at both ends to help with the ligation step. The protocol used is described below.

5.1.5.1 Introducing the NdeI and XhoI cut sites into the plasmid (insert)

1. Resuspend the primers with the NDEI and XHOI cut sites in Tris elution buffer to a final concentration of 100µM.
2. Make a 5ng/µl stock of the template.
3. Make the PCR sample as follows:
 - i. 10 µl of 5x reaction buffer
 - ii. 2 µl of 10µM forward mutant primer
 - iii. 2 µl of 10µM reverse mutant primer

- iv. 1.5 μl of 10mM dNTP mix
- v. 1 μl of 5 ng/ μl template
- vi. 2 μl of LongAmp Taq DNA polymerase
- vii. Bring to 50 μl with ddH₂O

Table 4. Polymerase chain reaction steps as programmed into thermocycler. This table shows the temperature, duration and number of cycles for each step in the PCR process.

Step	Temperature (°C)	Duration	# of cycles
First denaturation	95 °C	30 seconds	1
Denaturation	95 °C	30 seconds	30
Annealing	55 °C	30 seconds	
Extension	68 °C	8 minutes	
Last extension	68 °C	2 minutes	1
Hold	4 °C	————	————

Table 5. Restriction digest scheme. This table shows the quantities of all the reagents used in the digest of the vector and the PCR product (insert).

Vector	Vector + NDEI	Vector + XHOI	Sample	Insert
200ng of plasmid	200ng of plasmid	200ng of plasmid	1 μg of plasmid 1000ng= 1 μg	12 μl PCR product
1 μl of 10x reaction buffer 3	1 μl of 10x reaction buffer 3	1 μl of 10x reaction buffer 3	2 μl of 10x reaction buffer 3	2 μl 10x reaction buffer 3
Bring to 10 μl with H ₂ O	0.5 μl of NDEI	1 μl of XHOI	1 μl of NDEI	1 μl NDEI
	Bring to 10 μl with H ₂ O	Bring to 10 μl with H ₂ O	2 μl of XHOI	2 μl XHOI
			Bring to 20 μl with H ₂ O	

5.1.5.2 Digestion of the insert and pET28a vector using NDEI and XHOI

The PCR product and the pET28a vector were both digested by the restriction enzymes NDEI and XHOI. The digest was performed for 16hrs at 37°C on the vector and for 1hour at the same temperature for the insert.

After the digestion, the restriction enzymes were inactivated at 80°C for 20 minutes.

5.1.5.3 Agarose gel casting and sample extraction

A 2% 100 mL agarose gel was made using low melting temp agarose powder and TBE buffer. After the gel was made, gel loading dye was added to the digested samples from **Table 5**. The vector samples were loaded first, then run for about 30 minutes after which the run was paused, the insert was loaded, and the gel was run for another 40 minutes. The samples were extracted from the agarose gel using the GeneJET Gel Extraction Kit and manual from Thermo Scientific.

5.1.5.4 Ligation

The vector and insert were ligated following the steps below.

1. Add 2 µl T4 DNA ligase buffer to 3 centrifuge tubes.
2. Add 50ng of vector to each centrifuge tube.
3. Add 5.59ng of control insert to tube one. The control is an insert that has been previously for successful ligation.
4. Add 8.38ng of the PCR insert from the gel extraction to the second tube.
5. Do not add any insert to the third tube. This is a control.
6. Gently mix the contents of each tube.
7. Incubate the samples at 16°C overnight.
8. Transform into NEB 5α *E.coli* cells.

5.1.5.5 Transformation into NEB 5 α *E.coli* cells

1. Thaw the cells on ice.
2. Add 50 μ l of NEB 5 α *E.coli* cells to 3 sterile, labeled centrifuge tubes.
3. Add 5 μ l of the first sample from the ligation to the first tube.
4. Add 5 μ l of the second sample from the ligation to the second tube.
5. Add 5 μ l of the third sample from the ligation to the third tube.
6. Incubate the all the samples to be transformed on ice for 30 minutes.
7. Heat shock for 30 seconds in a water bath at 42°C.
8. Incubate on ice for 2 minutes.
9. Add 500 μ l of SOC rescue media.
10. Incubate in a shaking incubator at 225 RPM and 37°C for one hour.
11. Get agar plates with kanamycin that have been warmed to 37°C.
12. Plate 100 μ l of the controls on a kanamycin agar plate
13. Plate 100 μ l of the sample from step 4 on a kanamycin agar plate.
14. Incubate all the plates at 37°C overnight.
15. Store the plates at 4°C until they are ready to be used

5.1.6 Minipreps

Minipreparations (minipreps) of the plasmids made from the site-directed mutagenesis and sub-cloning were made from four isolated colonies on each plate, and the purified DNA was sent for sequencing to confirm that the mutation and sub-cloning worked properly.

5.1.6.1 Miniprep overnight cultures

Four to five individual colonies were picked from a freshly transformed plate and used to inoculate 5ml of LB media containing kanamycin in 5 separate 15ml falcon tubes. The samples

were incubated overnight at 37°C in a shaking incubator and then purified using the Thermo Scientific GeneJET Plasmid Miniprep Kit. The steps used are listed below.

- 1) Pellet the overnight cultures by centrifugation for 10 minutes at 5837g.
- 2) Keep the pellets on ice until you are ready to lyse them.
- 3) Add 250 µl of resuspension buffer containing RNase A to each falcon tube.
Resuspend the pellets in the buffer and make sure there are no clumps left. Let them sit for about 5 minutes.
- 4) Add 250 µl of lysis buffer and invert the tubes 4 to 6 times. This step should last no longer than 5 minutes.
- 5) Add 350 µl of neutralizing solution. Invert the tubes 4 to 6 times.
- 6) Centrifuge for 10 minutes at > 12000g to separate the soluble portion of the mix from the insoluble portion.
- 7) The plasmids are soluble, so the liquid portion contains the DNA.
- 8) Transfer the liquid portion into the mini columns provided in the kit without disturbing the solid portion and then centrifuge for 1 minute at > 12000g.
- 9) Add 500 µl of wash buffer containing ethanol then centrifuge at > 12000g
- 10) Repeat the wash step twice.
- 11) Centrifuge the mini columns without any buffer. This is to get rid of all the wash buffer and ethanol. Ethanol makes DNA less soluble, but the next major step requires the DNA to be soluble.
- 12) Let the columns sit open for about 10 minutes at room temperature.
- 13) Add 50 µl of elution buffer or FPLC H₂O, depending on the step after the miniprep.
- 14) Let it sit for 10 minutes before centrifuging for 2 minutes at > 12000g.

5.1.6.2 Measuring plasmid DNA concentration and purity

An ND1000 nanodrop spectrophotometer is used to measure the concentration of DNA in ng/ μ l at 260nm. The concentration should be at least 100ng/ μ l. The plasmid purity is also measured simultaneously using the ratios of the absorbance of the samples at various wavelengths. The 260nm / 230nm ratio estimates the contamination of the sample by organic solvents, and it should have a value > 2 to indicate a pure sample. The 260nm / 280nm ratio estimates the contamination of the sample by proteins, and a value > 1.8 indicates a clean sample. The samples that meet the concentration and purity criteria are sent to Eurofins MWG Operon for sequencing.

5.2 Expression and purification of COR15A WT and mutant proteins

5.2.1 Transformation into BL21 (DE3) *E.coli* cells

If the sequences sent to Operon come back correct, the plasmids are then transformed into competent BL21 (DE3) *E.coli* cells. The transformation process is described in section **5.1.2**.

5.2.2 Protein expression

Transformed *E.coli* cells as described in **5.1.2** that are less than a week old are incubated and expressed in M9 minimal media for subsequent lysis and purification. The cells are mostly expressed in 2L batches in M9 minimal media. The recipe for M9 media and the expression protocol are described below.

Making 2L M9 medium:

- 1) Start with 1.7L of H₂O
- 2) Add 200mL of 10X M9 salts
 - i. 12g of Na₂HPO₄
 - ii. 6g of KH₂PO₄

- iii. 1g of NaCl
 - iv. pH to ~ 7.1
- 3) Add 4 mL of 1 M MgSO₄
 - 4) Add 4 mL of 50mM CaCl₂
 - 5) Add 2 mL of 0.01 M FeCl₃
 - 6) Add 400 µL of 5mg/mL vitamin B1
 - 7) Add 4 grams of D-Glucose
 - 8) Adjust the pH of the solution mixture to 7.3 - 7.5
 - 9) Take out 2 mL from the 2L media and add it to a 15mL falcon tube. Label it “-N – Kan + cells”. This is the first control.
 - 10) Add 2g of ammonium chloride to the 2L media and take out 2ml. Add the 2ml to a 15ml falcon tube and label it “ +N – Kan + cells”. This is the second control.
 - 11) Quantity sufficient (Q.S) to 2L
 - 12) Filter sterilize using a bottle top filter into 2x 1L bottles
 - 13) Add 500 µl of 60mg/ml Kanamycin to each bottle. Shake well and take out 2ml. add the 2 mL sample to a 15 mL falcon tube and label it “ +N + Kan - cells” (This is the third control).

Make a 50 mL starter culture by taking out 50mL from the 2L media made, add it to a 250ml beveled conical flask and label it with the name of the protein it will be inoculated with. Using an inoculating loop, add the transformant colonies from the agar plate to the starter culture. Store the rest of the 2L media in an incubator at 37°C. Inoculate the first and second controls with the transformant colonies and place them in a shaking incubator at 37°C and ~150RPM, along with the starter culture. Leave the controls and starter culture in the incubator overnight (for at least 15-17 hours). The first and third controls should show no growth. The second control should show some growth. Check the OD₆₀₀ of the starter culture, and make sure it is well above 1. Based

on the OD_{600} of the starter culture calculate what volume of the starter culture is needed to start incubating the cells in 2x 1L M9 with a starting OD_{600} of 0.04. The 2X 1L cultures should be incubated in 2x 2800 mL beveled flasks in a shaking incubator at 37°C until the OD_{600} gets to ~0.55. The flasks should then be transferred to a shaking incubator set at 15°C until the OD_{600} gets to 0.6. Take out 300 μ L of the pre-induction sample, then induce the cultures with 1 mM IPTG. The cultures should be left at those conditions for 24hours. After the 24-hour expression period, take out 300 μ L, then pellet the cells 350 mL at a time at 11,280g for 5 minutes, then store in the freezer at -80°C until they are to be purified. Take out 300 μ L samples pre and post induction for SDS-PAGE analysis; then add 30 μ L of 6x Laemmli should be added to each one. The 24-hour expression period was established by performing an expression test on the proteins. For the expression test, 300 μ l of sample was taken out every 6 hours for a total of 24hours. Each sample was then spun down, the supernatant was removed, and the pellet was resuspended in 30 μ l of 6x Laemmli. The gel image below is for the expression test on the COR15A quadruple mutant (4G to A) and is representative of the expression for the other proteins used in this project (Figure 17).

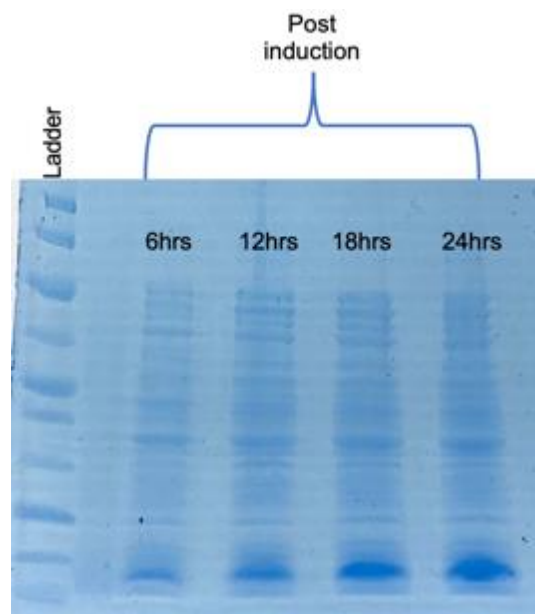


Figure 17. COR15A expression test. This figure shows the increase in expression of COR15A observed at 6hr time points for a total of 24hrs.

5.2.3 Purification protocol for COR15AWT and mutant

The two 1L pellets are fully resuspended in 25 mL of Nickel load buffer (the recipe is at the end of this paragraph) with one Pierce™ Protease inhibitor tablet per liter and lysed using a French cell pressure press. The lysed cells were then centrifuged at 38,000g for 1 hour to separate the soluble portion from the insoluble portion. The soluble portion of the lysate was then loaded at the rate of 2mL / minute onto a column containing ~35 mL of Ni-NTA resin connected to a Fast Protein Liquid Chromatography system. The desired protein has a 6x histidine tag that lets it stick to the resin in the column. The affinity column purification process is the first step towards getting the purified protein samples, and the protocol is in the next section below.

1) Recipe for Ni load/lysis buffer

- i. 50 mM sodium phosphate monobasic monohydrate
- ii. 300 mM sodium chloride (NaCl)
- iii. 10 mM imidazole
- iv. 0.02% sodium azide (NaN₃)
- v. pH 8

5.2.3.1 Nickel affinity column purification of COR15A WT and mutants

The first step is to equilibrate the nickel column with one column volume of nickel load buffer. The next step is to run nickel load buffer through the column at 3 mL / minute, which washes away any impurities that are not stuck to the column, then wash with ~50 mM elution to remove the impurities that have non-specifically bound to the column. The protein is then eluted with 2 column volumes of nickel elution buffer. The flow-through, wash, and elution step fractions are then run on an SDS-PAGE gel (**Figures 18 & 19**). COR15A pre-cleaved shows up at about 11 kDa on the SDS page gel (**Figure 19**). The elution fractions from the nickel column are pooled and dialyzed into gel filtration buffer (GFB). The GFB recipe is after **Figure 19**.

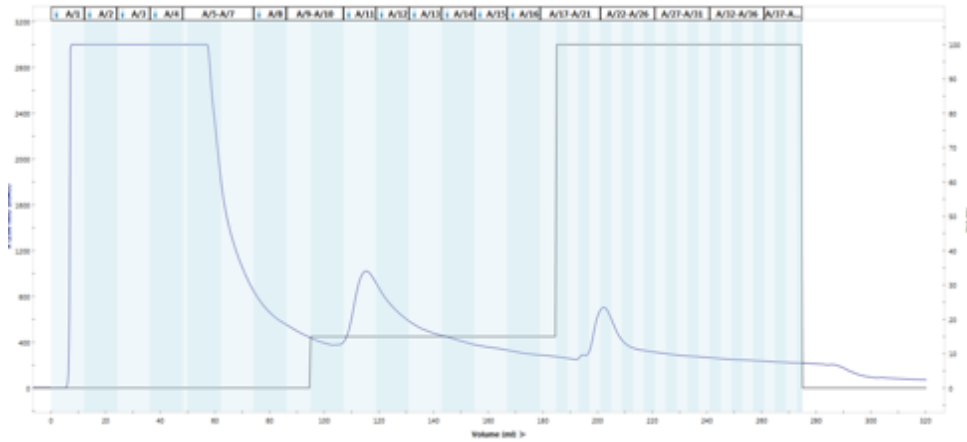


Figure 18. Nickel column chromatogram. This figure shows the chromatogram of 2L COR15AWT on a Biorad NGC FPLC system. The blue line and primary y-axis show the UV absorbance at each stage of the affinity purification process. The black line and secondary y-axis show the % of the elution buffer used in each step. The flow through peak is collected in fractions 1-10, the wash peak is collected in fractions 11-16 and the elution peak is collected in fractions 20-25.

2) Recipe for Nickel elution buffer

- i. 50 mM sodium phosphate monobasic monohydrate
- ii. 300 mM sodium chloride (NaCl)
- iii. 250 mM imidazole
- iv. 0.02% sodium azide (NaN_3)
- v. pH 8

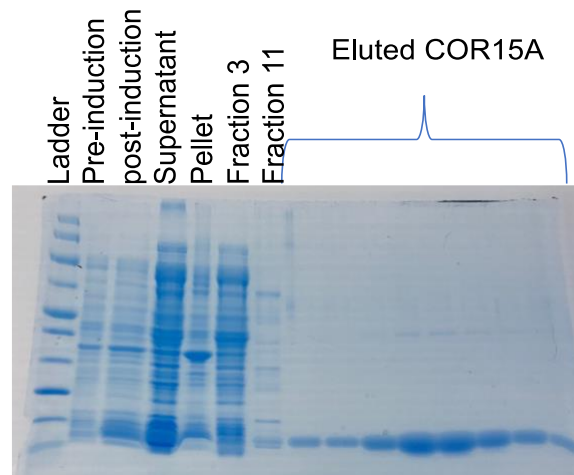


Figure 19. Nickel column fractions SDS-PAGE gel for COR15A WT. This gel shows the contents of the different fractions collected at different stages during the purification of COR15A WT using the nickel column

3) Gel filtration buffer (high salt phosphate buffer)

- i. 50 mM sodium phosphate monobasic monohydrate
- ii. 300 mM sodium chloride (NaCl)
- iii. 1 mM EDTA
- iv. 0.02% sodium azide (NaN₃)
- v. pH 7

5.2.3.2 Cleaving the 6x-histidine tag

After the protein was taken out of the dialysis buffer (high salt phosphate buffer), the 6x-histidine tag was cleaved using the Sigma Aldrich thrombin clean cleave kit. The thrombin beads had to be prepped first by washing them with GFB since the protein was dialyzed into GFB. The elution samples were analyzed on an SDS-PAGE gel, and it was seen that after 2 hours the tag was fully cleaved. This cleavage step leaves an overhang of about three residues, and the resulting protein is about 9.8 kDa (**Figure 23**). The cleaved protein was then dialyzed into anion

load buffer three times in preparation for the anion exchange column. The recipe for the anion load and elution buffers are below.

- 4) 2 L Anion load buffer
 - i. 20 mM Tris base
 - ii. 0.02% sodium azide
 - iii. pH 7
- 5) 1 L Anion exchange elution buffer
 - i. 20 mM Tris base
 - ii. 200 mM NaCl
 - iii. 0.02% sodium azide
 - iv. pH 7

5.2.3.3 Anion exchange chromatography

After the cleaved protein had been dialyzed into 3x 1L of anion load buffer it was loaded on the anion exchange column containing Q Sepharose™ High Performance resin by GE Healthcare. After the sample was run on the anion exchange column, the fractions were run on an SDS-PAGE gel, and the fractions containing the desired protein were pooled and concentrated down to just under 6 mL in preparation for the size exclusion (SEC) column.

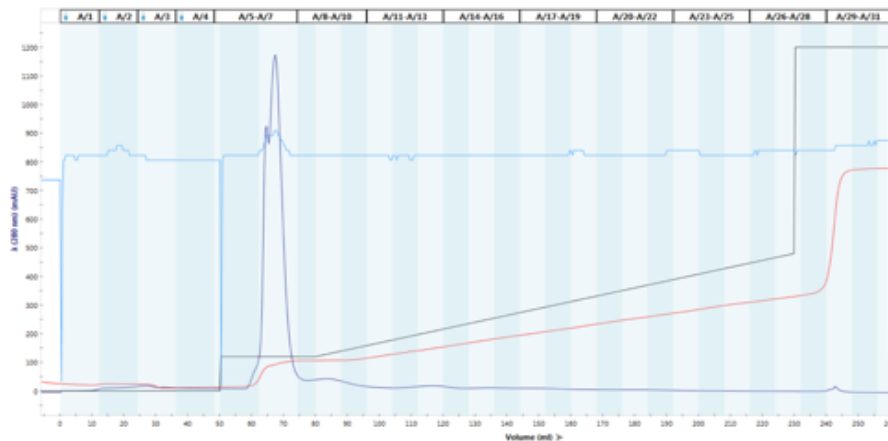


Figure 20. COR15A anion exchange chromatogram. This figure shows the chromatogram of 2L COR15AWT on a Biorad NGC FPLC system. The dark blue line and primary y-axis show the UV absorbance at each stage of the affinity purification process. The red line indicates the conductivity and the black line indicates the percentage of anion elution buffer. Most of the protein is in fraction 7.

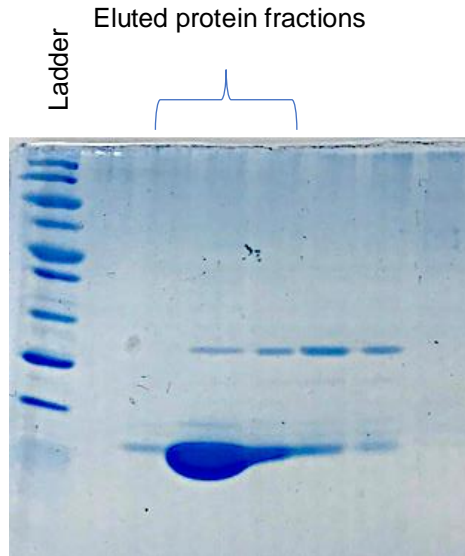


Figure 21. COR15A SDS-PAGE anion exchange gel. This figure shows the COR15A fractions from the anion exchange column. The column on the gel under the labeled eluted protein fractions were the ones that contained the desired protein.

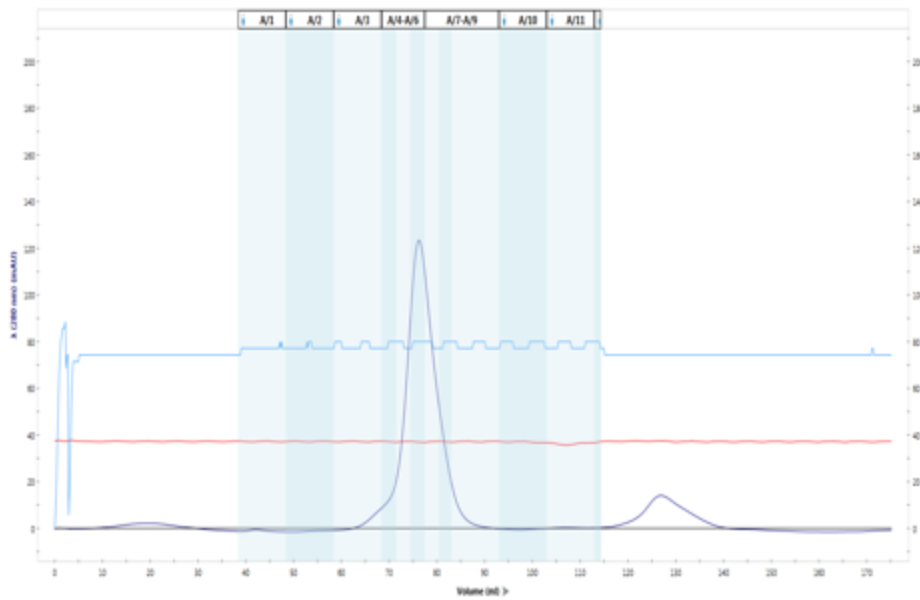


Figure 22. COR15A size exclusion chromatogram. This figure shows the chromatogram from the COR15A size exclusion step. The dark blue line and primary y-axis show the UV absorbance at each stage of the affinity purification process and the red line indicates the conductivity. COR15A is eluted in fractions 4-8.

5.2.3.4 Size exclusion (SEC) chromatography

This chromatography method separates the protein molecules based on their size (**Figure 22**). The resin used is the GE HiLoad 16/60 superdex 75, and the column volume is 120 mL. The resin beads have pockets which smaller molecules can flow into while they move through the column. Since only the smaller molecules get trapped in the pockets, the larger molecules are eluted first. The elution volume of COR15A is ~75 mL. The first step is to equilibrate the size exclusion column with ~1.25 column volumes of buffer. The protein sample is loaded and purified on the column 2 mL at a time at a buffer flow rate of 1 mL/minute. The fractions from the SEC are run on an SDS-PAGE gel, and the fractions corresponding to the purified protein are pooled and concentrated down to about 4 mL. The samples are stored at 4°C or -80°C depending on how long they need to be stored before they are used. If the samples are going to be used within a month, they are concentrated down to about 4ml and stored in a falcon tube in the fridge. If the samples are not going to be used within a month, they are concentrated to about 4ml and stored in cryo vials in the -80°C freezer.

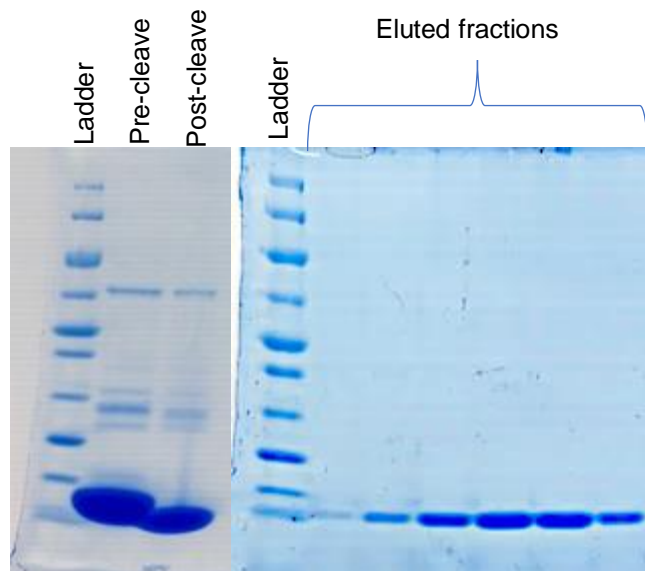


Figure 23. COR15A SDS-PAGE gel for the final stage of purification. These SDS-PAGE gels show COR15A before and after the histidine tag was cleaved, and the purified protein fractions.

5.3 Polyacrylamide gel electrophoresis (SDS-PAGE)

Sodium dodecyl sulfate polyacrylamide gel electrophoresis is a method of separation that separates protein molecules based on their size and charge. SDS is a detergent, and it gives the molecules a uniform charge because it has a net negative charge, and it evenly binds to the polypeptides. SDS is a detergent that breaks non covalent bonds, which means the samples are run under denaturing conditions.

The samples were run on an 8% to 20% gradient gel using 40% acrylamide solution with a ratio of acrylamide to bis-acrylamide of 29:1, and the electrophoresis power source was set to 190V for 45 minutes.

5.4 Determining protein concentration

The concentration of the WT and mutant proteins used for the NMR experiments were 300–500 μM . Protein concentration was measured using an ND1000 nanodrop. The extinction coefficient of COR15A is $2980 \text{ M}^{-1} \text{ cm}^{-1}$, which is quite low, so we tend to use the 280 nm absorbance data from more concentrated samples to estimate concentration. The lower detection limit of the Nanodrop U/V spectrophotometer used is 0.03 AU. For the NMR experiments, we usually work in the range of 100 μM and above, which gives an absorbance value of about 0.15AU, which is well above the sensitivity limit of the detector. All the protein samples used are diluted from concentrated protein stock solutions, and this method of measuring concentration is used consistently in all three proteins. The reliability of the COR15A protein concentrations calculated using UV absorbance was confirmed using BCA.

5.5 Nuclear magnetic resonance spectroscopy

The NMR experiments on the samples were carried out at 25°C on the Varian VNMRS 800 MHz spectrometer equipped with a triple resonance pulse field Z-axis gradient cold probe.

To make the amide ^1H and ^{15}N as well as $^{13}\text{C}_\alpha$ and $^{13}\text{C}_\beta$ resonance assignments, sensitivity enhanced ^1H - ^{15}N HSQC and three-dimensional HNCACB and HNCO experiments were performed on the uniformly ^{15}N -labeled and ^{15}N - and ^{13}C -labeled samples of COR15AWT and mutants in 90% H_2O , 10% D_2O , 50 mM NaH_2PO_4 , 50 mM NaCl , 1 mM EDTA, 0.02% NaN_3 , pH 6.8 for the samples without TFE. The samples with TFE (Trifluoroethanol) were in 70% H_2O , 20% TFE, 10% D_2O , 50 mM NaH_2PO_4 , 50 mM NaCl , 1 mM EDTA, 0.02% NaN_3 , pH 6.8. For the HNCACB and HNCO experiment, data were acquired in ^1H , ^{13}C , and ^{15}N dimensions using 9689.9228 (t3) X 14075.1787 (t2) X 1944.3904 (t1) Hz sweep widths, and 1024 (t3) X 128 (t2) X 32 (t1), respectively. For the HSQC experiments, the sweep width was 9689.9228 (t2) X 1944.3524 (t1), and the increments were 1024 (t2) and 128 (t1). The NMR spectra were taken with NMRFX Processor and analyzed using NMRViewJ (One Moon Scientific, Inc., Westfield, NJ, USA).

The data from the 2D and 3D NMR experiments were analyzed using the neighbor-corrected intrinsically disordered protein (NCIDP) random coil values and the Vendruscolo $\delta^2\text{D}$ software. The random coil values were included in the calculation of the alpha-carbon secondary chemical shifts, while the $\delta^2\text{D}$ software was used for the calculation of the % helix values [39, 40].

5.6 Circular Dichroism

Circular dichroism (CD) measurements were performed in a Jasco J-815 spectrometer (Jasco, Japan) equipped with a thermostatted, Peltier-controlled cell holder. Four spectra were recorded and averaged using quartz cuvettes with a path length of 1 mm (Hellma, Germany) at protein concentrations of 0.10 g/L in 10 mM NaH_2PO_4 pH 7.4 in the absence of co-solvent and with increasing concentrations of ethylene glycol (EG) or trifluoroethanol (TFE). All spectra were corrected for buffer contributions and converted to mean residue ellipticities $[\theta_{\text{MRW}}]$ using mean residue weights of 104.1 g/mol, 104.3 g/mol and 104.8 g/mol for COR15A WT, G68A and 4GtoA,

respectively. Instrument calibration was done with 1S-(+)-10-camphorsulphonic acid. The ratio of α -helix was estimated using θ MRW at 222 nm [27].

5.7 Carboxy fluorescein (CF) leakage assay

All lipids were purchased from Avanti Polar Lipids (Alabaster, AL, USA) and dissolved in chloroform prior to mixing in the respective ratio to model the lipid composition of inner chloroplast membranes (40% monogalactosyldiacylglycerol; 30% digalactosyldiacylglycerol; 15% sulfoquinovosyldiacylglycerol; 15% egg phosphatidylglycerol) referred to as ICMM [19]. A total of 10 mg of lipids was dried in a glass tube under a stream of N_2 at 60°C and subsequently under vacuum overnight to remove the solvent completely. Dry lipids were rehydrated in 100 mM carboxy fluorescein (CF); 10 mM TES, 50 mM NaCl and 0.1 mM EDTA, pH 7.4 as described previously [41, 42]. The mixture was vortexed for 5 s and resuspended multiple times over an interval of 15 min to resolve all the lipids, followed by extrusion through two layers of polycarbonate membranes with 100 nm pore size in a handheld extruder (Avanti Polar Lipids, Alabaster, AL, USA) for the formation of large unilamellar vesicles (LUVs). Liposomes were loaded onto a S75 13/300 size exclusion column connected to the Fast Protein Liquid Chromatography (FPLC) ÄKTA system (GE Healthcare, Freiburg, Germany) to remove free CF. Fractions containing liposomes were detected at 280 nm using the absorption of CF in the ultraviolet (UV) region. The hydrodynamic radius of the liposomes was measured by dynamic light scattering at a scattering angle of 90° with a custom-built apparatus, equipped with a 0.5 W diode-pumped continuous-wave laser (Cobolt Samba 532 nm, Cobolt AB, Solna, Sweden), a high quantum yield avalanche photo diode and an ALV 7002/USB 25 correlator (ALV-GmbH, Langen, Germany) at 23 °C. Hydrodynamic radii of liposomes were calculated from fits of the accumulated autocorrelation functions using the CONTIN algorithm implemented in a custom-made MatLab script (The Math-Works, Natick, MA, USA) [43].

Carboxy Fluorescein containing ICMM LUVs were mixed in equal volumes of respective protein solutions in final molar protein to lipid ratios ranging from 1:50 to 1:200 in polymerase chain reaction (PCR) tubes. Prior to this, protein concentrations were determined by ultraviolet/visible (UV/VIS) spectroscopy using the sequence-specific extinction coefficient at 280 nm of $2560 \text{ M}^{-1} \text{ cm}^{-1}$ valid for all three proteins [31]. Samples were rapidly frozen in an ethylene glycol bath precooled to $-20 \text{ }^{\circ}\text{C}$ for 2 h [32]. The frozen samples were thawed at $23 \text{ }^{\circ}\text{C}$ and transferred to 96-well fluorescent plates. CF leakage was determined with a VIROSKAN FLASH plate reader (Thermo Scientific, Waltham, MA, USA) using an excitation wavelength of 492 nm and an emission wavelength of 517 nm before and after disrupting the liposomes with Triton X-100 (Merck, Darmstadt, Germany). CF leakage from the liposomes was calculated as described previously and normalized to control ICMM LUVs which had not been subjected to a freeze-thaw cycle set as 0% leakage [33]. All proteins were tested for a significance level of $p < 0.001$ compared to ICMM LUVs without protein (w/o) or to COR15A WT, respectively in a one-way analysis of variance (ANOVA).

REFERENCES

1. van der Lee, R.; Buljan, M., et al. Classification of intrinsically disordered regions and proteins. *Chem Rev* **2014**. 114(13): 6589-6631. 10.1021/cr400525m
2. Uversky, V. N. Intrinsically disordered proteins and their environment: effects of strong denaturants, temperature, pH, counter ions, membranes, binding partners, osmolytes, and macromolecular crowding. *Protein J* **2009**. 28(7-8): 305-325. 10.1007/s10930-009-9201-4
3. Uversky, V. N. and Dunker, A. K. Understanding protein non-folding. *Biochim Biophys Acta* **2010**. 1804(6): 1231-1264. 10.1016/j.bbapap.2010.01.017
4. Brown, C. J.; Johnson, A. K., et al. Evolution and disorder. *Curr Opin Struct Biol* **2011**. 21(3): 441-446. 10.1016/j.sbi.2011.02.005
5. Murzin, A. G.; Brenner, S. E., et al. SCOP: a structural classification of proteins database for the investigation of sequences and structures. *J Mol Biol* **1995**. 247(4): 536-540. 10.1006/jmbi.1995.0159
6. Dunker, A. K.; Obradovic, Z., et al. Intrinsic protein disorder in complete genomes. *Genome Inform Ser Workshop Genome Inform* **2000**. 11: 161-171.
7. Hundertmark, M. and Hinch, D. K. LEA (late embryogenesis abundant) proteins and their encoding genes in *Arabidopsis thaliana*. *BMC Genomics* **2008**. 9: 118. 10.1186/1471-2164-9-118

- 8.Theillet, F. X.;Kalmar, L., et al. The alphabet of intrinsic disorder: I. Act like a Pro: On the abundance and roles of proline residues in intrinsically disordered proteins. *Intrinsically Disord Proteins* **2013**. 1(1): e24360. 10.4161/idp.24360
- 9.Romero, P.;Obradovic, Z., et al. Sequence complexity of disordered protein. *Proteins* **2001**. 42(1): 38-48.
- 10.Campen, A.;Williams, R. M., et al. TOP-IDP-scale: a new amino acid scale measuring propensity for intrinsic disorder. *Protein Pept Lett* **2008**. 15(9): 956-963.
- 11.Dunker, A. K.;Cortese, M. S., et al. Flexible nets. The roles of intrinsic disorder in protein interaction networks. *FEBS J* **2005**. 272(20): 5129-5148. 10.1111/j.1742-4658.2005.04948.x
- 12.Dunker, A. K.;Garner, E., et al. Protein disorder and the evolution of molecular recognition: theory, predictions and observations. *Pac Symp Biocomput* **1998**. 473-484.
- 13.Fukuchi, S.;Homma, K., et al. Intrinsically disordered loops inserted into the structural domains of human proteins. *J Mol Biol* **2006**. 355(4): 845-857. 10.1016/j.jmb.2005.10.037
- 14.Hsu, W. L.;Oldfield, C. J., et al. Exploring the binding diversity of intrinsically disordered proteins involved in one-to-many binding. *Protein Sci* **2013**. 22(3): 258-273. 10.1002/pro.2207
- 15.Dunker, A. K.;Brown, C. J., et al. Intrinsic disorder and protein function. *Biochemistry* **2002**. 41(21): 6573-6582.
- 16.Uversky, V. N. Natively unfolded proteins: a point where biology waits for physics. *Protein Sci* **2002**. 11(4): 739-756. 10.1110/ps.4210102
- 17.Wishart, D. S. Interpreting protein chemical shift data. *Prog Nucl Magn Reson Spectrosc* **2011**. 58(1-2): 62-87. 10.1016/j.pnmrs.2010.07.004

18. Kleckner, I. R. and Foster, M. P. An introduction to NMR-based approaches for measuring protein dynamics. *Biochim Biophys Acta* **2011**. 1814(8): 942-968.
10.1016/j.bbapap.2010.10.012
19. Thalhammer, A.; Bryant, G., et al. Disordered cold regulated 15 proteins protect chloroplast membranes during freezing through binding and folding, but do not stabilize chloroplast enzymes in vivo. *Plant Physiol* **2014**. 166(1): 190-201.
10.1104/pp.114.245399
20. Popova, A. V.; Hundertmark, M., et al. Structural transitions in the intrinsically disordered plant dehydration stress protein LEA7 upon drying are modulated by the presence of membranes. *Biochim Biophys Acta* **2011**. 1808(7): 1879-1887.
10.1016/j.bbamem.2011.03.009
21. Candat, A.; Paszkiewicz, G., et al. The ubiquitous distribution of late embryogenesis abundant proteins across cell compartments in Arabidopsis offers tailored protection against abiotic stress. *Plant Cell* **2014**. 26(7): 3148-3166. 10.1105/tpc.114.127316
22. Tunnacliffe, A., H., D.K., Leprince, O., Macherel, D. (2010). LEA Proteins: Versatility of Form and Function. C. J. Lubzens E., Clark M. Berlin, Heidelberg, Springer. **21**: 91-108.
23. Hinch, D. K. and Thalhammer, A. LEA proteins: IDPs with versatile functions in cellular dehydration tolerance. *Biochem Soc Trans* **2012**. 40(5): 1000-1003.
10.1042/BST20120109
24. Colmenero-Flores, J. M.; Moreno, L. P., et al. Pvlea-18, a member of a new late-embryogenesis-abundant protein family that accumulates during water stress and in the growing regions of well-irrigated bean seedlings. *Plant Physiol* **1999**. 120(1): 93-104.

25. Thalhammer, A.; Hundertmark, M., et al. Interaction of two intrinsically disordered plant stress proteins (COR15A and COR15B) with lipid membranes in the dry state. *Biochim Biophys Acta* **2010**. 1798(9): 1812-1820. 10.1016/j.bbamem.2010.05.015
26. Navarro-Retamal, C.; Bremer, A., et al. Molecular dynamics simulations and CD spectroscopy reveal hydration-induced unfolding of the intrinsically disordered LEA proteins COR15A and COR15B from *Arabidopsis thaliana*. *Phys Chem Chem Phys* **2016**. 18(37): 25806-25816. 10.1039/c6cp02272c
27. Steponkus, P. L.; Uemura, M., et al. Mode of action of the COR15a gene on the freezing tolerance of *Arabidopsis thaliana*. *Proc Natl Acad Sci U S A* **1998**. 95(24): 14570-14575.
28. Artus, N. N.; Uemura, M., et al. Constitutive expression of the cold-regulated *Arabidopsis thaliana* COR15a gene affects both chloroplast and protoplast freezing tolerance. *Proc Natl Acad Sci U S A* **1996**. 93(23): 13404-13409.
29. Navarro-Retamal, C.; Bremer, A., et al. Folding and Lipid Composition Determine Membrane Interaction of the Disordered Protein COR15A. *Biophys J* **2018**. 115(6): 968-980. 10.1016/j.bpj.2018.08.014
30. Dosztanyi, Z. Prediction of protein disorder based on IUPred. *Protein Sci* **2018**. 27(1): 331-340. 10.1002/pro.3334
31. Dosztanyi, Z.; Csizmok, V., et al. IUPred: web server for the prediction of intrinsically unstructured regions of proteins based on estimated energy content. *Bioinformatics* **2005**. 21(16): 3433-3434. 10.1093/bioinformatics/bti541

- 32.Chen, Y. H.;Yang, J. T., et al. Determination of the secondary structures of proteins by circular dichroism and optical rotatory dispersion. *Biochemistry* **1972**. 11(22): 4120-4131.
- 33.Sreerama N, W. R. Estimation of protein secondary structure from circular dichroism spectra: Comparison of CONITIN, SELCON, and CDSSTR methods with an expanded reference set. *Analytical Biochemistry* **2000**. 2017(287(2)): 252-260.
- 34.Buck, M. Trifluoroethanol and colleagues: cosolvents come of age. Recent studies with peptides and proteins. *Q Rev Biophys* **1998**. 31(3): 297-355.
- 35.Bakaltcheva, I., Schmitt JM, Hinch DK. . Time- and temperature dependent solute loading of isolated thylakoids during fr. *Cryobiology* **1992**. 29(5): 607-615.
- 36.Contreras-Martos, S.;Nguyen, H. H., et al. Quantification of Intrinsically Disordered Proteins: A Problem Not Fully Appreciated. *Front Mol Biosci* **2018**. 5: 83. 10.3389/fmolb.2018.00083
- 37.Nakayama, K.;Okawa, K., et al. Arabidopsis Cor15am is a chloroplast stromal protein that has cryoprotective activity and forms oligomers. *Plant Physiol* **2007**. 144(1): 513-523. 10.1104/pp.106.094581
- 38.Bremer, A.;Kent, B., et al. Intrinsically Disordered Stress Protein COR15A Resides at the Membrane Surface during Dehydration. *Biophys J* **2017**. 113(3): 572-579. 10.1016/j.bpj.2017.06.027
- 39.Camilloni, C.;De Simone, A., et al. Determination of secondary structure populations in disordered states of proteins using nuclear magnetic resonance chemical shifts. *Biochemistry* **2012**. 51(11): 2224-2231. 10.1021/bi3001825

40. Tamiola, K.; Acar, B., et al. Sequence-specific random coil chemical shifts of intrinsically disordered proteins. *J Am Chem Soc* **2010**. 132(51): 18000-18003. 10.1021/ja105656t
41. Hinch, D. K. Release of two peripheral proteins from chloroplast thylakoid membranes in the presence of a Hofmeister series of chaotropic anions. *Arch Biochem Biophys* **1998**. 358(2): 385-390. 10.1006/abbi.1998.0866
42. Oliver, A. E.; Hinch, D. K., et al. Interactions of arbutin with dry and hydrated bilayers. *Biochim Biophys Acta* **1998**. 1370(1): 87-97.
43. Provencher, S. W. CONTIN: A general purpose constrained regularization program for inverting noisy linear algebraic and integral equations. *Computer Physics Communication* **1982**. 27(issue 3): 229-242.

APPENDICES

Appendix A: Chemical shifts tables for COR15AWT and mutants

Table A1. COR15AWT 0%TFE chemical shifts

Residue	AA	HA	CA	CB	CO	N	HN
1	M	0	0	0	0	0	0
2	A	0	52.3888	19.19	177.2994	0	0
3	A	0	52.37455	19.4175	177.8015	123.8471	8.28201
4	K	0	56.4302	33.10406	177.2127	121.0501	8.30794
5	G	0	45.39304	0	173.9435	110.243	8.39557
6	D	0	54.36834	41.38906	176.8814	120.4974	8.22843
7	G	0	45.5117	19.15948	173.9948	109.1097	8.40545
8	N	0	53.31533	39.05564	175.2206	118.9235	8.31915
9	I	0	61.49854	38.82847	176.2116	121.4395	8.12517
10	L	0	55.23169	42.25946	177.0951	125.6825	8.27745
11	D	0	54.68932	41.33057	176.0721	121.3316	8.16716
12	D	0	54.61279	41.20572	176.7072	120.5877	8.21577
13	L	0	55.85227	41.98376	177.688	122.3771	8.18962
14	N	0	53.83015	39.05564	175.7321	118.9235	8.31915
15	E	0	57.42593	30.09482	176.9012	121.3327	8.30987
16	A	0	53.48879	19.10326	178.6799	123.5696	8.25792
17	T	0	62.62781	69.48206	174.9322	112.4398	7.95452
18	K	0	56.74362	33.01316	176.6275	123.7631	8.05079
19	K	0	56.34538	33.17083	176.6233	122.5167	8.27142
20	A	0	52.9908	19.269	178.1789	125.3438	8.31116
21	S	0	58.62167	63.73287	174.3966	114.4182	8.21528
22	D	0	54.58873	41.07324	175.852	122.0052	8.19124
23	F	0	57.99117	39.58752	175.5915	119.9996	8.0012
24	V	0	62.4337	32.93809	176.0637	122.3902	7.98409
25	T	0	62.06672	69.77767	174.1772	118.1324	8.17932
26	D	0	54.38953	41.11967	176.6144	123.032	8.32436
27	K	0	56.8393	32.78686	177.3847	122.6578	8.381944
28	T	0	63.03393	69.51981	175.0837	114.6994	8.21094
29	K	0	56.88632	32.88918	176.9737	122.7716	8.10758
30	E	0	57.00291	30.27481	176.4218	121.6085	8.23574
31	A	0	52.6494	19.13776	177.9094	124.7107	8.178654
32	L	0	55.23156	42.40717	177.487	121.2784	8.09461
33	A	0	52.62566	19.32775	177.7161	124.8249	8.23881
34	D	0	54.88343	41.21016	177.1114	119.7297	8.25578

35	G	0	45.65311	0	174.5245	109.196	8.28176
36	E	0	56.6615	30.36426	176.7654	120.6638	8.18432
37	K	0	56.27935	33.12081	176.4564	122.0052	8.19124
38	A	0	52.98203	19.17747	177.7361	125.4046	8.35946
39	K	0	56.54556	33.10406	176.2961	120.7842	8.314444
40	D	0	54.25867	41.10077	175.626	120.6638	8.18432
41	Y	0	57.90552	38.86827	175.2894	120.3519	7.92081
42	V	0	62.23794	33.06651	175.5611	123.5578	7.95548
43	V	0	62.3503	32.85193	176.058	124.7512	8.11434
44	E	0	56.54961	30.41901	176.3025	125.5481	8.44087
45	K	0	56.46997	33.06385	176.3004	123.1841	8.37448
46	N	0	53.4053	39.05907	175.3639	120.5018	8.53837
47	S	0	58.74817	63.75382	174.7061	116.584	8.34627
48	E	0	56.90226	30.28849	176.8386	122.8146	8.49118
49	T	0	61.81576	69.82584	174.4785	114.6592	8.13298
50	A	0	52.96934	19.3745	177.7066	126.3662	8.30737
51	D	0	54.6481	41.18068	176.7976	119.6183	8.33431
52	T	0	62.38477	69.51841	175.0866	114.1422	8.05044
53	L	0	55.88968	42.18909	178.2699	123.9761	8.20268
54	G	0	45.67969	0	174.649	109.7779	8.42972
55	K	0	56.69427	33.03228	177.3341	121.0194	8.11131
56	E	0	57.39263	29.81987	176.7852	121.6595	8.53529
57	A	0	52.883	19.14492	178.4264	124.6937	8.26346
58	E	0	57.20914	30.11856	177.102	119.9219	8.23254
59	K	0	57.0774	32.9627	176.638	122.0396	8.15464
60	A	0	52.8988	19.09666	177.9198	124.5976	8.19957
61	A	0	52.83878	19.12942	178.0065	122.9924	8.12781
62	A	0	53.00897	19.10923	177.5092	122.8356	8.18333
63	Y	0	58.16278	38.82187	175.5893	119.8946	8.01356
64	V	0	62.31227	33.15331	175.6134	123.5175	7.84429
65	E	0	56.76061	30.41682	176.5425	124.8858	8.29879
66	E	0	56.8402	30.37848	176.7042	123.358	8.43036
67	K	0	56.82309	32.78686	177.5475	122.7407	8.39035
68	G	0	45.57871	0	174.3152	110.0776	8.50083
69	K	0	56.2588	33.0753	177.0739	121.0448	8.1074
70	E	0	57.14041	29.97486	177.0462	121.64	8.47273
71	A	0	53.09631	19.0501	177.9198	124.3832	8.2332
72	A	0	52.83878	19.12942	177.9844	122.967	8.12689
73	N	0	53.39452	38.70004	175.5832	117.6469	8.26573

74	K	0	56.23	32.92448	176.4592	122.0302	8.16202
75	A	0	52.67984	19.32775	177.6953	124.8773	8.23229
76	A	0	52.66504	19.1846	177.9983	122.5971	8.06369
77	E	0	57.05977	30.28772	176.5106	119.6265	8.18526
78	F	0	57.71835	39.50854	175.6391	120.4111	8.11921
79	A	0	52.63858	19.47658	177.5296	125.477	8.09634
80	E	0	56.92396	30.26978	177.1823	120.032	8.28564
81	G	0	45.49823	0	174.649	109.9056	8.35211
82	K	0	56.69427	33.046	176.7489	121.0448	8.11036
83	A	0	52.8003	19.16453	178.3584	124.6384	8.1632
84	G	0	45.34098	0	174.1629	108.3513	8.33012
85	E	0	56.36261	30.61	176.3983	120.6449	8.14811
86	A	0	52.70438	19.17747	177.9218	125.6206	8.36498
87	K	0	56.51846	33.03234	176.384	120.5877	8.21577
88	D	0	54.27061	41.21169	175.9894	121.2382	8.29987
89	A	0	52.67984	19.39112	177.9461	124.8212	8.224749
90	T	0	62.17619	69.80555	173.8223	113.5803	8.22776
91	K	0	57.69423	33.80126	0	128.8004	7.83796

Table A2. COR15AWT 20%TFE chemical shifts

Residue	AA	HA	CA	CB	CO	N	HN
1	M	0	0	0	0	0	0
2	A	0	0	0	177.1926	0	0
3	A	0	52.43168	19.31528	177.5348	122.8863	8.13226
4	K	0	56.3793	33.18849	177.0534	119.8642	8.16408
5	G	0	45.37552	0	173.837	109.6424	8.33016
6	D	0	54.32061	41.24273	176.7811	120.1731	8.18957
7	G	0	45.57217	0	173.9756	108.6884	8.37336
8	N	0	53.32776	39.1877	175.6302	119.0018	8.37482
9	I	0	62.60091	38.5621	176.294	121.1368	8.03936
10	L	0	56.38588	41.61521	178.0602	122.1396	7.98397
11	D	0	56.16483	40.889	177.3609	119.9706	7.92814
12	D	0	55.97823	40.72248	177.8512	120.279	8.0199
13	L	0	57.01563	41.8878	178.7294	121.9697	8.21926
14	N	0	55.39969	38.71633	176.8339	119.2448	8.3411
15	E	0	58.78376	29.63947	177.8512	120.4114	8.23926
16	A	0	54.79	18.3379	179.7149	121.9697	8.21926
17	T	0	64.68047	69.14179	176.1354	111.6889	8.04077

18	K	0	58.5144	32.53239	177.7398	123.3341	7.8655
19	K	0	57.94804	32.65796	178.0267	119.5709	8.08034
20	A	0	54.25	18.36	178.6927	122.6783	8.09138
21	S	0	60.21188	63.21498	175.9929	112.9895	8.09147
22	D	0	56.1211	40.60905	176.7518	122.6171	8.27522
23	F	0	59.80473	39.37659	176.5129	120.0203	7.95736
24	V	0	64.58807	29.90169	177.776	119.5096	8.04928
25	T	0	64.51315	69.21798	175.1399	117.7326	8.21973
26	D	0	56.36865	40.72893	177.9134	122.3883	8.26687
27	K	0	57.47583	31.78394	178.5602	120.4114	8.26126
28	T	0	65.2945	68.93437	175.6363	115.6279	8.11852
29	K	0	59.06713	32.34362	178.2815	121.1611	8.02996
30	E	0	58.58733	29.90509	177.6181	119.4692	8.00265
31	A	0	53.95566	18.39485	179.413	122.4329	7.90225
32	L	0	56.24776	42.11369	178.3189	118.9853	7.99957
33	A	0	53.6086	18.6725	178.5447	122.6433	7.91924
34	D	0	55.37943	41.11068	177.6036	118.8727	8.08811
35	G	0	46.1585	0	175.1226	108.5244	8.20581
36	E	0	57.62346	29.92221	177.4871	120.6041	8.14731
37	K	0	57.18764	32.78659	177.111	120.2208	7.99627
38	A	0	53.32893	18.89182	178.226	122.7897	8.00772
39	K	0	57.51722	32.63782	176.6696	118.6918	7.88876
40	D	0	55.15092	40.8598	176.3515	119.3599	8.03007
41	Y	0	58.81029	38.63557	175.8297	119.6843	7.8382
42	V	0	63.59579	32.60492	176.3861	120.9016	7.8259
43	V	0	63.60462	32.53659	176.8389	122.356	7.95734
44	E	0	57.44216	30.09302	177.0775	123.4094	8.28765
45	K	0	56.81292	32.59367	176.9425	121.4744	8.252138
46	N	0	53.95247	38.97947	175.6516	119.363	8.37457
47	S	0	59.53946	63.59994	174.9833	116.0743	8.22097
48	E	0	57.70803	30.04521	177.4851	122.4616	8.40286
49	T	0	63.0987	69.61209	174.8914	114.56	8.08464
50	A	0	53.9682	18.95432	178.593	124.8275	8.21555
51	D	0	55.5211	41.09279	177.3536	118.649	8.24533
52	T	0	64.19918	69.27929	175.7	114.6742	7.99108
53	L	0	57.0647	41.88955	178.8918	122.8038	8.22831
54	G	0	46.45647	0	175.7224	107.959	8.33352
55	K	0	57.96603	32.34362	178.7056	121.1182	8.01504
56	E	0	58.83012	29.10642	178.5244	120.2771	8.37838

57	A	0	54.83178	18.0224	179.8112	122.8038	8.22831
58	E	0	59.09035	29.73252	178.8549	118.6176	8.05188
59	K	0	58.89465	32.50022	178.3781	120.3238	7.88982
60	A	0	54.29673	18.09298	179.7373	122.3933	8.05057
61	A	0	54.55254	18.18698	179.7373	120.5877	8.21577
62	A	0	54.55254	18.18698	179.553	120.5877	8.21577
63	Y	0	60.72861	38.33991	177.1566	120.0171	8.01458
64	V	0	65.88783	32.14153	178.4407	119.5002	8.10933
65	E	0	58.91251	29.66133	178.5751	121.2554	8.09824
66	E	0	58.827	29.6741	178.9011	120.5048	8.17113
67	K	0	57.60543	31.3451	179.4203	119.9595	8.34586
68	G	0	46.53585	0	175.9713	108.6884	8.37336
69	K	0	58.81363	32.53659	178.3811	122.356	7.95734
70	E	0	58.83117	29.8824	178.3538	120.3335	8.1209
71	A	0	54.3847	18.2906	179.5089	122.1546	8.08736
72	A	0	54.38158	18.21069	179.55	121.109	8.01239
73	N	0	55.12928	38.53901	176.9503	117.4223	8.16532
74	K	0	58.02116	32.21392	177.9511	120.8466	8.09593
75	A	0	54.29673	18.2088	179.2042	122.3371	8.06579
76	A	0	54.13705	18.39473	179.0904	121.1566	7.91163
77	E	0	58.27736	29.89351	177.9595	118.6184	8.01039
78	F	0	58.93188	39.14483	176.7302	119.5096	8.04928
79	A	0	53.64949	18.89182	178.4708	123.2389	8.02343
80	E	0	57.44456	30.02097	177.6656	118.4706	8.14283
81	G	0	45.79516	0	174.7874	108.5088	8.14383
82	K	0	56.36506	32.80498	176.7884	120.4265	7.97094
83	A	0	53.14673	18.93522	178.4305	124.0579	8.16663
84	G	0	45.44556	0	174.2985	107.2449	8.19765
85	E	0	56.64814	30.51739	176.4742	120.4026	8.06673
86	A	0	52.74601	18.95432	177.8298	124.686	8.22497
87	K	0	56.58753	33.04967	176.3526	120.1621	8.15309
88	D	0	54.32061	41.24273	176.0145	120.6059	8.19498
89	A	0	52.82652	19.24361	177.8364	124.3073	8.13967
90	T	0	62.11161	69.8098	173.7039	112.4594	8.14683
91	K	0	57.6328	33.82744		128.1954	7.70132

Table A3. COR15 G68A 0%TFE chemical shifts

Residue	AA	HA	CA	CB	CO	N	HN
1	M	0	0	0	0	0	0
2	A	0	52.33356	19.36081	177.3011	0	0
3	A	0	52.33356	19.36081	177.7805	123.8409	8.27947
4	K	0	56.38877	33.07621	177.2197	121.0016	8.302252
5	G	0	45.34823	0	173.9442	110.2413	8.39339
6	D	0	54.565	41.1426	176.8831	120.5057	8.226644
7	G	0	45.45402	0	173.9987	109.0994	8.40334
8	N	0	53.29278	38.72923	175.2225	118.9219	8.31682
9	I	0	61.46994	38.72923	176.2164	121.4429	8.1242
10	L	0	55.20139	42.19495	177.0975	125.6751	8.27528
11	D	0	54.65963	41.29642	176.0811	121.3306	8.1653
12	D	0	54.565	41.1426	176.7321	120.5486	8.21214
13	L	0	55.81525	41.91193	177.6958	122.3791	8.18853
14	N	0	53.83376	38.9911	175.7416	118.9219	8.31682
15	E	0	57.39122	30.0623	176.9094	121.3555	8.308522
16	A	0	53.44104	18.99855	178.6941	123.5472	8.25597
17	T	0	62.61458	69.4545	174.9403	112.4258	7.95083
18	K	0	56.70406	32.94308	176.6408	123.7572	8.04614
19	K	0	56.28305	33.11567	176.6332	122.4985	8.26796
20	A	0	52.96725	19.15126	178.1618	125.334	8.30877
21	S	0	58.58303	63.7087	174.3988	114.4244	8.21342
22	D	0	54.54874	41.04008	175.8586	122.0258	8.1881
23	F	0	57.917	39.53414	175.5971	120.0148	7.99729
24	V	0	62.4045	32.87569	176.0653	122.3887	7.98226
25	T	0	62.02999	69.75243	174.1826	118.1314	8.17717
26	D	0	54.36643	41.06384	176.5709	123.0323	8.32255
27	K	0	56.85549	32.62752	177.3872	122.7226	8.39873
28	T	0	62.99643	69.47832	175.0905	114.6947	8.2095
29	K	0	56.83813	32.83667	176.9742	122.7531	8.10634
30	E	0	56.91496	30.19908	176.4051	121.6081	8.23417
31	A	0	52.62792	19.04141	177.9098	124.6318	8.17613
32	L	0	55.20145	42.36666	177.5016	121.2906	8.0909
33	A	0	52.63119	19.2827	177.7198	124.8267	8.23073
34	D	0	54.83222	41.13931	177.1147	119.7458	8.25399
35	G	0	45.60992	0	174.4969	109.1878	8.27997
36	E	0	56.6315	30.32391	176.7829	120.6626	8.18214

37	K	0	56.30113	33.06349	176.5145	122.0035	8.18857
38	A	0	52.7682	19.25625	177.7805	125.3842	8.35075
39	K	0	56.38877	33.07621	176.3004	120.7813	8.310893
40	D	0	54.2254	41.03569	175.6315	120.6758	8.18152
41	Y	0	57.86784	38.82158	175.2944	120.3492	7.91935
42	V	0	62.19169	33.01052	175.5624	123.5612	7.95333
43	V	0	62.32035	32.80191	176.0653	124.7471	8.11211
44	E	0	56.52145	30.36813	176.3101	125.5475	8.43954
45	K	0	56.36191	33.11042	176.3044	123.1759	8.37286
46	N	0	53.36415	39.00523	175.3703	120.5003	8.53626
47	S	0	58.71672	63.7251	174.7127	116.5822	8.34538
48	E	0	56.88671	30.19879	176.8496	122.8137	8.48967
49	T	0	61.78433	69.78532	174.4925	114.6539	8.1326
50	A	0	52.94065	19.28784	177.7471	126.3298	8.30641
51	D	0	54.62837	41.10709	176.8218	119.6011	8.33416
52	T	0	62.43748	69.47633	175.1421	114.1993	8.04987
53	L	0	55.92874	42.14669	178.3545	123.9245	8.20621
54	G	0	45.68319	0	174.7735	109.7341	8.42899
55	K	0	56.85092	32.81308	177.4863	121.0061	8.12302
56	E	0	57.55531	29.68014	177.2497	121.5205	8.5349
57	A	0	53.2559	18.79682	178.6911	124.2803	8.2348
58	E	0	57.41114	30.00406	177.3563	119.8756	8.22648
59	K	0	56.93119	32.81594	177.4994	121.8323	8.12668
60	A	0	53.33952	18.89447	178.4199	124.4422	8.16925
61	A	0	53.06977	18.89418	178.1423	122.515	8.10869
62	A	0	53.06977	18.89418	177.9648	122.8084	8.12428
63	Y	0	58.751	38.60667	175.9826	119.8499	7.9848
64	V	0	63.13696	32.86217	176.3569	122.7248	7.83083
65	E	0	57.36741	30.08069	177.1494	124.275	8.2342
66	E	0	57.59944	30.05175	177.55	122.7226	8.39873
67	K	0	57.11658	32.48672	177.3735	121.6178	8.25502
68	A	0	53.06187	18.89447	178.9016	124.45	8.17
69	K	0	57.46528	32.81308	177.5099	120.6429	8.14358
70	E	0	57.41816	30.2545	177.1529	121.1329	8.19176
71	A	0	53.13128	18.89447	178.1124	123.9284	8.16751
72	A	0	53.01109	18.94585	178.3544	122.6831	8.08119
73	N	0	53.67802	38.58423	175.8627	117.7137	8.22623
74	K	0	56.93119	32.81594	175.9926	121.8323	8.12668
75	A	0	52.63119	19.2827	178.1124	124.8267	8.23073

76	A	0	52.94691	19.01003	178.1213	122.3159	8.07205
77	E	0	57.1262	30.16629	176.6511	119.5385	8.14397
78	F	0	57.76215	39.41897	175.7466	120.3042	8.105129
79	A	0	52.66366	19.40186	177.6286	125.31	8.07609
80	E	0	56.9099	30.16891	177.2143	119.9339	8.27129
81	G	0	45.48117	0	174.3095	109.8282	8.33571
82	K	0	56.06349	33.06823	176.9328	120.9805	8.09568
83	A	0	52.82519	19.12611	178.3657	124.2851	8.15005
84	G	0	45.27517	0	174.172	108.3299	8.32684
85	E	0	56.34801	30.57226	176.3704	120.6429	8.14358
86	A	0	52.55996	19.11743	177.9201	125.621	8.363
87	K	0	56.45656	32.95316	176.3865	120.5078	8.212895
88	D	0	54.2605	41.13838	176.4656	121.1942	8.294346
89	A	0	52.63119	19.2827	177.9535	124.8349	8.23028
90	T	0	62.14048	69.76915	173.8268	113.5815	8.22636
91	K	0	57.65772	33.72574	0	128.7984	7.836

Table A4. COR15 G68A 20%TFE chemical shifts

Residue	AA	HA	CA	CB	CO	N	HN
1	M	0	0	0	0	0	0
2	A	0	52.43359	19.24757	177.2275	0	0
3	A	0	52.43359	19.24757	177.5592	122.8328	8.13972
4	K	0	56.33798	33.29928	177.0773	119.8086	8.17497
5	G	0	45.35205	0	173.8766	109.6538	8.34907
6	D	0	54.31199	41.20385	176.8215	120.2521	8.21192
7	G	0	45.52581	0	174.0071	108.6506	8.39329
8	N	0	53.3139	39.18863	175.7215	119.0372	8.40566
9	I	0	62.71135	38.57508	176.3496	121.1544	8.05987
10	L	0	56.53749	41.52313	178.2391	121.8535	7.98133
11	D	0	56.3462	40.81399	177.5772	119.9016	7.92811
12	D	0	56.11953	40.59752	178.1885	120.4343	8.032
13	L	0	57.13884	41.84173	178.958	122.0034	8.26027
14	N	0	55.56956	38.74224	177.0112	119.3748	8.38233
15	E	0	58.8825	29.55188	177.9894	120.3492	8.25146
16	A	0	54.93401	18.22029	179.8808	121.9611	8.25441
17	T	0	64.91659	69.04346	176.3335	111.7676	8.09264
18	K	0	58.70705	32.424	178.3206	123.4703	7.88865
19	K	0	58.26977	32.51565	178.3296	119.5516	8.08934

20	A	0	54.38383	18.24751	178.8073	122.5116	8.11492
21	S	0	60.45741	63.14371	176.3283	112.9373	8.12651
22	D	0	56.29499	40.47444	176.9386	122.86	8.33352
23	F	0	60.09284	39.31549	176.7005	120.3173	7.9886
24	V	0	64.94973	32.20779	178.1625	119.1568	8.13738
25	T	0	64.90591	69.02564	175.3158	117.9122	8.27282
26	D	0	57.13884	40.60596	178.1711	122.4255	8.28483
27	K	0	57.46981	31.61495	178.7964	120.1943	8.28559
28	T	0	65.60339	68.83463	175.7215	115.9396	8.15167
29	K	0	59.30215	32.31818	178.4851	121.1838	8.05859
30	E	0	58.70032	29.86411	177.786	119.3678	7.99652
31	A	0	54.04087	18.41928	179.677	122.3331	7.91028
32	L	0	56.35453	42.04388	178.4883	118.8689	8.03841
33	A	0	53.72675	18.59847	178.7271	122.4987	7.92739
34	D	0	55.45924	41.06683	177.73	118.8607	8.10415
35	G	0	46.20794	0	175.2454	108.5146	8.2256
36	E	0	57.69805	29.8447	177.6349	120.6519	8.16319
37	K	0	57.21004	32.80602	177.2639	120.1991	7.99025
38	A	0	53.40424	18.66829	178.3203	122.6194	8.01369
39	K	0	57.67169	32.5564	176.8097	118.567	7.88239
40	D	0	55.24017	40.80005	176.517	119.2281	8.03834
41	Y	0	58.89928	38.5878	175.9669	119.6895	7.85869
42	V	0	63.76097	32.52505	176.5754	120.7219	7.85002
43	V	0	63.76592	32.47309	177.0158	122.1411	7.98073
44	E	0	57.55979	30.02035	177.2423	123.2381	8.30019
45	K	0	56.81475	32.47786	177.1081	121.2948	8.27155
46	N	0	53.86789	38.91164	175.7672	119.3748	8.38233
47	S	0	59.64589	63.52771	175.087	116.0879	8.24109
48	E	0	57.80802	29.95797	177.6658	122.4719	8.41699
49	T	0	63.33812	69.53808	174.9961	114.7122	8.10887
50	A	0	54.13196	18.867	178.7979	124.8739	8.22938
51	D	0	55.64426	41.08051	177.4931	118.5948	8.26122
52	T	0	64.46226	69.23613	175.8332	114.8335	8.01482
53	L	0	57.1785	41.8209	179.0255	122.7582	8.26855
54	G	0	46.52999	0	175.9446	107.7581	8.3503
55	K	0	58.06496	32.25328	178.9457	121.0747	8.01329
56	E	0	58.92332	28.99579	178.7165	120.2306	8.37268
57	A	0	54.97429	17.8392	179.9396	122.7582	8.26855
58	E	0	59.26826	29.71494	179.1021	118.4828	8.06037

59	K	0	59.10209	32.49471	178.5825	120.2423	7.89768
60	A	0	54.8486	17.8697	179.1021	122.3987	8.07865
61	A	0	54.76826	17.92946	179.9743	120.2171	7.89702
62	A	0	54.76826	17.92946	180.0317	120.3293	7.9045
63	Y	0	61.09501	38.25284	177.4516	120.3402	8.032
64	V	0	66.66071	31.6374	178.7678	119.3243	8.21045
65	E	0	59.41579	29.33438	0	119.6843	8.0616
66	E	0	59.49672	29.2804	179.6132	0	0
67	K	0	57.7735	30.94574	179.5364	119.6836	8.20766
68	A	0	55.0756	17.62918	180.5258	124.0626	8.52897
69	K	0	59.37775	32.51565	178.9868	119.5	8.08908
70	E	0	59.30359	29.8671	178.8735	120.3556	8.05859
71	A	0	54.95622	17.8697	180.033	121.8944	8.10214
72	A	0	54.71395	17.85886	180.0893	121.2896	8.11412
73	N	0	55.58262	38.52142	177.4055	117.5888	8.20374
74	K	0	58.26502	32.02249	178.3407	120.6554	8.13937
75	A	0	54.54073	17.9805	179.5173	122.12	8.0903
76	A	0	54.32901	18.22968	179.361	120.9869	7.91893
77	E	0	58.51373	29.82599	177.9088	118.5946	8.00763
78	F	0	59.29523	39.05399	177.0098	119.5683	8.08934
79	A	0	53.84174	18.73484	178.7175	122.9703	8.06212
80	E	0	57.53117	29.9148	177.8472	118.2832	8.15092
81	G	0	45.86372	0	174.9667	108.3616	8.13831
82	K	0	56.36951	32.67648	176.9167	120.383	7.97898
83	A	0	53.2486	18.8904	178.5331	123.9216	8.16646
84	G	0	45.45071	0	174.387	107.1298	8.20478
85	E	0	56.68614	30.45221	176.5574	120.4239	8.07563
86	A	0	52.75578	18.867	177.9478	124.6166	8.23169
87	K	0	56.61338	33.0868	176.4131	120.1201	8.15839
88	D	0	54.31199	41.20385	176.0701	120.5973	8.20898
89	A	0	52.89537	19.21251	177.8881	124.2842	8.15482
90	T	0	62.1099	69.79428	173.7385	112.4108	8.16303
91	K	0	57.59115	33.77954	0	128.1992	7.71209

Table A5. COR15 4GtoA 0%TFE chemical shifts

Residue	AA	CA	CB	CO	N	HN
1	M	0	0	0	0	0
2	A	0		177.326828	0	0
3	A	52.3961716	19.1923809	178.094528	123.812309	8.27480984
4	K	56.5332489	33.1084709	177.222092	121.07019	8.30955982
5	G	45.3813782		173.95541	110.225372	8.39587975
6	D	54.3783913	41.3508911	176.898331	120.55933	8.23415
7	G	45.5068703		174.020157	109.12989	8.41254044
8	N	53.3923492	39.0438919	175.248352	118.95047	8.32861042
9	I	61.5014992	38.6854782	175.650894	121.721222	8.13566971
10	L	55.2445602	42.2416	177.12918	125.7015	8.28641033
11	D	54.58538	41.31994	176.09999	121.33862	8.1744
12	D	54.61367	41.20094	176.72118	120.65523	8.21735
13	L	55.8273811	41.9395103	177.704544	122.37282	8.19464
14	N	53.846199	39.0438919	175.730408	118.95047	8.32861042
15	E	57.3929787	30.1129894	176.891998	121.368973	8.32034969
16	A	53.4300194	19.1772194	178.679596	123.635406	8.26821041
17	T	62.6196098	69.4994965	174.943588	112.504158	7.9660902
18	K	56.7399788	33.0234413	176.647766	123.786774	8.06585026
19	K	56.3273888	33.1614914	176.636612	122.551826	8.2826004
20	A	52.9926605	19.2198391	178.184525	125.363953	8.32098007
21	S	58.6189194	63.7442894	174.414047	114.411789	8.2218399
22	D	54.5998802	41.0890808	175.870056	122.001198	8.20055008
23	F	57.938221	39.5921707	175.60936	120.024727	8.00459957
24	V	62.438591	32.9252281	176.099136	122.388977	7.99077988
25	T	62.0478096	69.7885666	174.206985	118.131279	8.18630981
26	D	54.4024391	41.1090698	176.583374	123.038338	8.33218002
27	K	56.8568993	32.6885185	177.408493	122.730698	8.39406967
28	T	63.0209312	69.5072632	175.1035	114.721786	8.21664047
29	K	56.8756714	32.879631	177.003128	122.781197	8.11728001
30	E	57.0680313	30.23979	176.95889	121.61731	8.24590015
31	A	52.6733284	19.1663208	177.924881	124.9008	8.18116
32	L	55.2335396	42.3982391	177.507996	121.298889	8.09990978
33	A	52.6525002	19.2406292	177.743301	124.887039	8.23933983
34	D	54.9011993	41.2072601	177.138351	119.837463	8.26076984
35	G	45.6443291		174.53401	109.21637	8.28934956
36	E	56.58045	30.3053	176.72118	120.67338	8.1938

37	K	56.4337	33.10511	176.24522	122.0012	8.20055
38	A	52.34262	19.40474	177.75902	125.7015	8.28641
39	K	56.53325	33.10847	176.30673	120.78836	8.31268
40	D	54.2582703	41.0739594	175.659897	120.67338	8.1938
41	Y	57.9161186	38.8548889	175.320358	120.345734	7.9261198
42	V	62.2649307	33.1130981	175.591339	123.521797	7.9608798
43	V	62.365799	32.8338814	176.102875	124.733627	8.11985016
44	E	56.57267	30.4032898	176.353897	125.531837	8.44766045
45	K	56.4295006	33.12463	176.349777	123.192177	8.38381958
46	N	53.4374008	39.0298119	175.426361	120.456543	8.54708958
47	S	58.7943611	63.7624397	174.754623	116.632088	8.35787964
48	E	57.0731812	30.2409306	177.028259	122.87291	8.49590015
49	T	62.1179619	69.8246231	174.692673	114.774834	8.17691994
50	A	53.383461	19.1381092	178.235901	125.959923	8.33339977
51	D	55.1208801	41.0891113	177.158829	119.547867	8.34012985
52	T	63.5685997	69.3141785	175.509964	115.222076	8.04485035
53	L	56.399189	41.9354782	178.3546	123.601227	8.16345024
54	A	53.49996	18.79709	178.95499	124.11336	8.12033
55	K	57.435	32.65907	177.75902	120.03587	8.11424
56	E	57.68702	29.7779	177.72354	121.07095	8.3157
57	A	53.2170982	19.1556091	178.293411	123.93215	8.1787
58	E	57.02285	30.1306992	177.747238	120.034363	8.23841
59	K	57.4780006	32.8288193	121.52519	121.525192	8.0630703
60	A	53.49996	18.79709	178.70169	123.93215	8.12288
61	A	53.42606	18.82101	178.51749	122.50509	8.11123
62	A	53.1908607	18.8821602	178.221878	122.64663	8.08667
63	Y	59.0150795	38.5685501	176.190659	119.813057	7.97202015
64	V	63.5100212	32.7131004	176.667648	122.285812	7.8302598
65	E	57.5719414	30.0847301	177.378189	123.661636	8.21354961
66	E	57.8621712	30.0336609	177.82033	122.756317	8.39103985
67	K	57.06803	32.45556	177.72688	121.36225	8.25057
68	A	53.6402	18.6937	179.13437	121.36225	8.25057
69	K	57.69579	32.75327	177.66707	120.65623	8.13586
70	E	57.67053	30.34057	177.72354	121.03862	8.1764
71	A	53.78079	18.68554	178.70169	123.95006	8.18091
72	A	53.33197	18.83552	178.621246	122.64663	8.08667
73	N	53.9013405	38.5525894	176.10945	117.887451	8.24615955
74	K	57.1899	32.6416	177.14212	121.7435	8.15049
75	A	53.40525	18.78751	178.39919	123.93215	8.13788

76	A	53.26159	18.83555	178.47908	122.10234	8.03837
77	E	57.6441498	30.1105194	177.145432	119.747353	8.1534996
78	F	58.2545891	39.3484917	176.035156	120.36515	8.1209898
79	A	53.2299194	19.2309895	176.42795	124.619743	8.06445026
80	E	56.61078	30.33111	177.07063	119.84485	8.1713
81	A	52.7802	19.11782	178.39279	125.01014	8.1826
82	K	56.56736	32.82068	176.47929	120.3316	8.16241
83	A	52.9422112	19.0791607	178.074844	125.0887	8.23934
84	A	52.9422112	19.0960808	178.1707	122.862083	8.16267967
85	E	56.7037582	30.3649807	176.04814	119.757347	8.17350006
86	A	52.6771011	19.1556091	177.938431	125.0887	8.23934
87	K	56.5804482	33.0903893	176.517044	120.655228	8.21735001
88	D	54.3819084	41.2011604	176.427948	121.074509	8.26471996
89	A	52.780201	19.1178207	177.989639	124.64621	8.19128036
90	T	62.1611519	69.8215866	173.845261	113.487556	8.21541023
91	K	57.7040482	33.7606201		128.83096	7.83918

Table A6. COR15 4GtoA 20%TFE chemical shifts

Residue	AA	HA	CA	CB	CO	N	HN
1	M	0	0	0	175.63965	0	0
2	A	0	52.49989	19.2725	177.232803	124.93788	8.2231
3	A	0	52.4233704	19.3186302	178.906723	123.032944	8.16903019
4	K	0	56.4370613	33.164341	177.098648	119.646744	8.20442963
5	G	0	45.3709602	0	173.874863	109.74836	8.35962963
6	D	0	54.3365402	41.2885895	176.82869	120.233177	8.2132597
7	G	0	45.5194511	0	173.995438	108.76123	8.39846992
8	N	0	53.3202591	39.1693192	175.583786	119.008369	8.38261986
9	I	0	62.3688583	38.9295692	176.29747	121.169563	8.07787991
10	L	0	56.1228485	41.7513695	177.866333	122.755379	8.0606699
11	D	0	55.8667107	41.0077705	177.108368	120.244728	7.98692989
12	D	0	55.6835403	40.7574005	177.625076	120.338097	8.07812977
13	L	0	56.8043289	41.8862	178.532639	122.093246	8.22679043
14	N	0	55.1153297	38.7800407	176.698074	119.126984	8.34521008
15	E	0	58.5458984	29.7020798	177.858978	120.611488	8.28022003
16	A	0	54.6005096	18.4447899	179.587189	122.093246	8.2347002
17	T	0	64.2965088	69.1738586	175.936508	111.748802	8.0329504
18	K	0	58.2141418	32.6171188	177.38214	123.299896	7.89525986
19	K	0	57.5710983	32.8475304	177.770752	119.94041	8.12304

20	A	0	53.9772682	18.6070194	178.60672	123.041054	8.12629032
21	S	0	59.8981514	63.3081512	175.630905	113.171532	8.11176014
22	D	0	55.7374992	40.6557999	176.588104	122.426109	8.27070999
23	F	0	59.3797188	39.4309807	176.3195	119.890022	7.97626019
24	V	0	64.05026	32.52107	177.364624	120.04272	8.0087
25	T	0	64.0299835	69.2717896	174.966125	117.682701	8.21613979
26	D	0	55.8563309	40.7361794	177.64899	122.429466	8.30428028
27	K	0	57.37447	31.99932	178.34264	120.8348	8.29822
28	T	0	64.8275986	69.1200027	176.260147	115.271507	8.14148045
29	K	0	58.5851593	32.4801216	178.09258	121.386963	8.04452038
30	E	0	58.29247	29.96049	177.404587	119.8588	8.06239
31	A	0	53.666729	18.6351204	179.095581	122.720802	7.95336008
32	L	0	55.9981689	42.1603012	178.115433	119.243378	7.99971008
33	A	0	53.4191589	18.6351204	178.348251	123.027809	7.98400021
34	D	0	55.2358589	41.1310616	177.49704	119.011513	8.12436962
35	G	0	46.0218086	0	175.007996	108.660667	8.23946953
36	E	0	57.4157791	30.0125198	177.345963	120.607323	8.18056011
37	K	0	56.9397011	32.8353882	176.956314	120.41748	8.03567028
38	A	0	53.1601486	18.9172096	178.494095	123.127258	8.05710983
39	K	0	57.1789398	32.8071709	176.605606	119.335983	7.93725014
40	D	0	54.8961105	40.8920212	176.177582	119.556473	8.07886982
41	Y	0	58.5482407	38.6666908	175.708771	119.707527	7.85961008
42	V	0	63.2452507	32.6894989	176.214081	121.301353	7.8505702
43	V	0	63.2765503	32.5902786	176.672287	122.762733	7.99014997
44	E	0	57.2346382	30.1472397	176.921387	123.715469	8.33981037
45	K	0	56.77631	32.6494598	176.797974	121.764603	8.28686047
46	N	0	53.862751	38.8831406	175.696976	119.548553	8.42601967
47	S	0	59.5663986	63.574749	175.056824	116.210648	8.28761959
48	E	0	57.9093704	29.9397507	177.794525	122.607094	8.45989037
49	T	0	63.6591187	69.5066833	175.122192	115.138519	8.17026043
50	A	0	54.5536919	18.5465698	179.064819	124.554962	8.26268005
51	D	0	56.16502	41.0755806	177.76881	118.513527	8.26051998
52	T	0	65.5053406	68.9743423	175.537643	115.954498	8.02035999
53	L	0	57.7440605	41.6785011	179.076492	122.478416	8.22336006
54	A	0	54.8896103	17.9689407	180.25113	122.008141	8.08106995
55	K	0	58.61538	32.19483		118.54328	7.96344
56	E	0	58.8987083	29.0681705	178.976791	120.27487	8.24662
57	A	0	55.02528	17.7994194	180.17986	123.018646	8.28227997
58	E	0	59.17196	29.72968	179.13651	119.06567	8.03252

59	K	0	59.12278	32.52544		120.39104	7.9
60	A	0	54.88961	17.96894	180.11806		
61	A	0	54.75921	17.96894	179.21519	121.51838	8.12122
62	A	0	54.73813	18.0609	178.90157	120.51442	7.94334
63	Y	0					
64	V	0					
65	E	0	59.41854	29.35019	178.7435		
66	E	0	59.41854	29.35019	179.57941	119.94511	8.12987
67	K	0	57.7976189	30.9999504		119.656273	8.20246029
68	A	0	55.03899	17.7373905		124.0214	8.44419003
69	K	0					
70	E	0	59.2497	29.81644	178.85638		
71	A	0	54.88961	17.96894	180.53275	121.9358	8.11367
72	A	0	54.89196	17.89934	180.237869	119.94978	8.09166
73	N	0	55.7433205	38.3779182	177.53757	118.133926	8.26790047
74	K	0	58.44438	31.94722	178.53673	120.855347	8.19845963
75	A	0	54.88961	17.96894	179.93123	122.149788	8.11406994
76	A	0	54.71831	18.11226	179.8024	121.591454	7.99029016
77	E	0	59.01689	29.81732	177.589569	119.332573	8.11007023
78	F	0	59.9782791	38.9422493	177.031326	120.24012	8.21070957
79	A	0	54.8002586	18.2139492	180.15683	122.096878	8.16748047
80	E	0	58.6100693	29.5991993	178.350113	118.861526	8.18192005
81	A	0	54.4681206	18.0571003	180.02536	123.475616	8.02184963
82	K	0	57.40379	31.78062	175.639648	118.72028	8.15062
83	A	0	53.90793	18.4183	179.21519	123.02781	7.9906
84	A	0	53.90793	18.4183	179.09596	121.11094	7.9312
85	E	0	57.69481	30.15989	177.383331	118.73046	7.9024
86	A	0	53.240551	18.6964607	178.166534	122.697868	7.90670013
87	K	0	57.2426682	32.7348289	176.898132	119.012062	7.96397018
88	D	0	54.6943016	41.1780014	176.242523	120.385918	8.10291958
89	A	0	52.9026794	19.2207108	178.020416	123.738029	8.05988979
90	T	0	62.1100883	69.7873917	173.753708	112.316292	8.09445
91	K	0	57.6852913	33.7294884		128.389786	7.70939016

APPENDIX B: COPYRIGHT INFORMATION

Note . From “Conserved Glycines Control Disorder and Function in the Cold-Regulated Protein COR15A,” by Sowemimo O.T, Knox-Brown P., Borchers W., Rindfleisch T., Thalhammer A., Daughdrill G.W., 2019, 9(3), 84; <https://doi.org/10.3390/biom9030084>

Open Access Article

Conserved Glycines Control Disorder and Function in the Cold-Regulated Protein, COR15A

by Oluwakemi T. Sowemimo, Patrick Knox-Brown, Wade Borchers, Tobias Rindfleisch, Anja Thalhammer and Gary W. Daughdrill

Biomolecules **2019**, 9(3), 84; <https://doi.org/10.3390/biom9030084>

Received: 15 January 2019 / Revised: 15 February 2019 / Accepted: 25 February 2019 / Published: 2 March 2019

Viewed by 135 | [PDF Full-text](#) (1350 KB)

Abstract Cold-regulated (COR) 15A is an intrinsically disordered protein (IDP) from *Arabidopsis thaliana* important for freezing tolerance. During freezing-induced cellular dehydration, COR15A transitions from a disordered to mostly α -helical structure. We tested whether mutations that increase the helicity of COR15A also increase its protective [...] [Read more](#).

(This article belongs to the Special Issue [Intrinsically Disordered Proteins and Chronic Diseases](#))